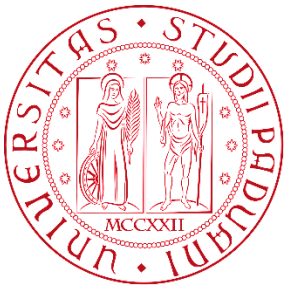

UNIVERSITY OF PADOVA

Department of General Psychology

Padova Neuroscience Center

Master's degree in Cognitive Neuroscience and Clinical Neuropsychology

Final dissertation

Dynamic activity patterns and cortico-subcortical interactions in the human brain

Supervisor

Professor Antonino Vallesi

Co-supervisor

Dottor Michele Allegra, PhD

***Candidate*:** Alessandro Nazzi

***Student ID number*:** 2038703

Academic Year 2022-2023

INDEX

0. ABSTRACT

The mechanisms underlying the dynamic patterns of connectivity observed in spontaneous brain activity remain poorly understood. In this thesis work, we present additional evidence indicating that the fluctuations in cortical activity within the ultra-slow frequency range (<0.01–0.1 Hz) are contingent upon interactions with subcortical areas. Utilizing functional magnetic resonance imaging (fMRI) data derived from resting-state conditions included in the Human Connectome Project's database, we identified what we refer to as Dynamic Functional States (DFSs) – transient, yet recurrent groupings of cortical and subcortical regions that synchronize at ultra-slow frequencies. We noticed that shifts in cortical groupings occur concurrently with shifts in subcortical groupings, demonstrating that cortical regions display flexible synchronization with either limbic regions (such as the hippocampus and amygdala) or subcortical nuclei (including the thalamus and basal ganglia). We corroborate our claims by carefully scrutinizing the validity of theoretical assumptions underlying dynamic functional connectivity with a particular focus on the stationarity debate. Finally, we provide some hints regarding the intriguing relationship between interindividual differences in resting state connectivity patterns and behavior.

1. INTRODUCTION

1.1. Intrinsic activity

In the last decade, there has been a paradigm shift in the study of brain function, spotlighting resting-state activity (or intrinsic activity) in the infra-slow frequency range (< 0.1 Hz), in spite of task-evoked activity. While the study of task-related activity increase has been extremely fruitful at all levels of research in neuroscience, it tends to encourage a reactive view of brain activity. An alternative view, however, considers brain function as mainly intrinsic, open-ended and explicitly oriented to interpreting, responding to and predicting environmental necessities. A growing portion of the literature suggests that this different conception is more consistent with brain's functional organization (Raichle, 2010), as well as its asymmetric allocation of energy resources (Howarth et al., 2012; Harris et al., 2012).

1.1.1. What is a resting state?

First of all, given the restless and complex nature of the brain, it might be useful to clarify what we refer to when we talk about resting-state activity. In humans, the resting state is defined as a behavioral state, characterized by neural activity fluctuations in the absence of a specific task. We can assume that, during this state, subjects undergo a state of conscious awareness, distinguished by stimulus-independent thoughts. Discriminating between the behavioral definition of the resting state and the actual brain state during rest is crucial. The brain in fact, never experiences a physiological state of rest, as evident from its intrinsic activity and its high energy consumption, which remains relatively stable

whether at rest or engaged in attention-demanding tasks (Sokoloff et al., 1955; Petersen et al., 1988).

1.1.2. Energy consumption

The imbalance between the brain and the rest of the body in terms of energy consumption is a striking metabolic evidence: even though our brain constitutes around 2% of the body's weight, it contributes to more than 20% of the total energy consumption (Mink et al., 1981). The energetic cost of our nervous system depends on the levels of cellular oxidative metabolism, supplying the essential energy for functioning in form of ATP. This metabolic cost is relatively constant between active and resting states, and this stability is common across different domains of brain activity. The direct consequence is that the brain's energy supply sets a rigid boundary for mental processing capacities. Therefore, when there is heightened neural activity due to increased mental task demands, compensatory reductions in cellular metabolism are needed elsewhere (Bruckmaier et al., 2020).

Regarding the details of energy consumption, it has been long thought that most of the cortical energy use was dedicated to the propagation of action potentials (i.e., around 47% of the total energy expenditure) due to the necessity of maintaining a sufficient Na^+ influx to compensate for the simultaneous K^+ currents flowing out of the cell (through the functioning of active sodium-potassium pumps). However, mammalian neurons turned out to be much more energy efficient than previously thought (Alle et al., 2009; Carter and Bean, 2009). Revising the neurons' metabolic needs in light of this recent discovery

allowed to uncover that the majority of energy use is now predicted to be on synaptic transmission, accounting for 59% of the total energy use (including postsynaptic receptors 50%, presynaptic Ca2+ entry, vesicle cycling 5% and neurotransmitter recycling 4%) (Howarth et al., 2012). Consequently, the actual amount of energy consumed by action potentials accounts for 21%. This neurobiological piece of information adds up to the growing evidence highlighting the functional and behavioral importance of resting-state activity.

1.1.3. Meaning of the intrinsic activity

While most fMRI studies implicitly assume that the functional connectivity between brain regions remains constant over time in task-free experiments, it appears that the long-time average correlation of infra-slow activity (the so-called static FC), emerges on top of rapidly switching connectivity patterns, the so-called dynamic FC or dFC (Hutchison et al., 2013). Even though the functional significance of intrinsic brain activity remains largely unknown, it appears to be behaviorally relevant.

A promising clue about the functional implications of spontaneous brain activity comes from the clinical literature. Evidence from different clinical domains and pathologies reveal correlations between abnormalities in intrinsic functional connectivity and behavioral impairments (Baldassarre et al., 2016). Additionally, spontaneous activity patterns are reported to covary with individual differences in cognitive functions and to be influenced by learning (Smith et al., 2015; Albert et al. 2009). A stimulating view about spontaneous activity in cortical and subcortical networks suggests that top-down computational

processes, allowing generative models to learn and infer states of the world, might be a promising way of interpreting dFC at rest (Pezzulo et al., 2021). In this sense, low-frequency transitions in spontaneous activity would allow our brain to orchestrate generic priors, explore its dynamic repertoire and regularize the complexity of its internal generative models. Moreover, this model aggregates two disjointed components of resting state activity: low-frequency spontaneous activity and high-frequency replays. In fact, the latter might integrate the functional impact of the former by selectively updating the model with fictive data represented in terms of high-frequency transitions. These transitions, known as replays, occur in different brain regions such as the visual and prefrontal cortex, even though their most typical location of study resides in the hippocampus, where they manifest as reactivations of previously experienced connectivity patterns (Foster, 2017).

This perspective supports an emerging framework emphasizing the pivotal role of spontaneous brain activity in cognition. According to this view, the learning process begins with preexisting circuit dynamics that generate spontaneous activity, which is initially meaningless. However, over time, this activity gains meaning by aligning itself with the statistical and dynamic patterns of the external world through actions and perception of their consequences. While task-related activity is influenced by external inputs, spontaneous activity during periods of rest reveals manifestations of the internal model, which appears to prepare us for future interactions.

1.2. Connectivity dynamics and states

This intrinsic activity is spatio-temporally organized in Intrinsic Connectivity Networks (ICNs), which are a set of spatially distributed and temporally correlated brain regions (Damoiseaux et al., 2006). ICNs clearly emerge from the study of temporal correlation, or functional connectivity (FC) in functional magnetic resonance imaging (fMRI), and they appear to be strongly related to the underlying structural connectivity (Damoiseaux and Greicius, 2009).

1.2.1. Main Resting State Networks

A key issue related to the study of brain connectivity regards the definition criteria and the taxonomy associated with macro-scale functional networks. Even though a clear understanding of what constitutes a large-scale neurocognitive network is still lacking in the literature, a widespread and homogeneously accepted naming convention might avail the heterogeneous field of network neuroscience.

A promising strategy for network definition relies on the study of resting-state functional connectivity (RSFC, see methods) paired with the examination of task co-activation patterns through meta-analysis. A potential universal taxonomy was proposed by Uddin et al. (2019). In their work they focus on cortical areas, presenting a taxonomy system divided into six macro-scale networks defined as: Occipital, Pericentral, Dorsal, Lateral and Medial Frontoparietal and Mid-cingulo-insular network, each comprising 1-2 core regions and associated with a cognitive label. The Occipital network (ON) includes both striate and extra-striate occipital cortices as well as the lateral geniculate nucleus and is

consequently devoted to visual information processing (Fig. 1a). The Pericentral network (PN) is involved in motor and somatosensory processes and includes as core regions the motor and somatomotor cortices, localized respectively posteriorly and anteriorly to the central sulcus. The PN network also comprises the supplementary motor area (Fig. 1b). The Dorsal portion of the Frontoparietal network (D-FPN) is constituted by the superior parietal lobule also including the intraparietal sulcus, middle temporal cortex, ventral premotor cortex and the frontal eye field areas. It is generally involved in visuospatial attention and top-down selection for stimuli and responses (Fig. 1c). Core regions of the Lateral Frontoparietal network (L-FPN) are lateral, rostral and dorsolateral prefrontal cortices as well as anterior inferior parietal lobule. This network also includes the intraparietal sulcus and mid-cingulate gyrus. The L-FPN is functionally active in goal-oriented cognition, working memory, inhibition and task switching (i.e., executive functions) with a particular focus on the control of information flow in the brain (Fig. 1d). The Midcingulo-insular network (M-CIN) comprises the anterior midcingulate cortex and bilateral anterior insula. Its functions pertain to salience processing, with the detection of behaviorally relevant environmental stimuli (Fig. 1e). Finally, the core regions of the Medial Frontoparietal network (M-FPN), also known as Default Mode Network (DMN), are medial prefrontal cortex, posterior cingulate cortex and the posterior part of the inferior parietal lobule. Additionally, M-FPN also includes the inferior frontal gyrus, middle temporal gyrus, superior temporal sulcus and parahippocampal cortex. Despite a general lack of consensus about its functions, this network is likely involved in the formation, temporal binding and dynamic reconfiguration of associative representations based on current goal-sets as well as mind-wandering and autobiographical memory (Fig. 1f).

For the sake of reproducibility, in this study we employ the same networks' nomenclature adopted by Favaretto and colleagues (2022): roughly, the 'visual' network aligns with the ON, the 'sensorimotor' network with the PN, the 'dorsal attention' network with the D-FPN, the 'ventral attention' network with the M-CIN, the 'control' network with the L-FPN.

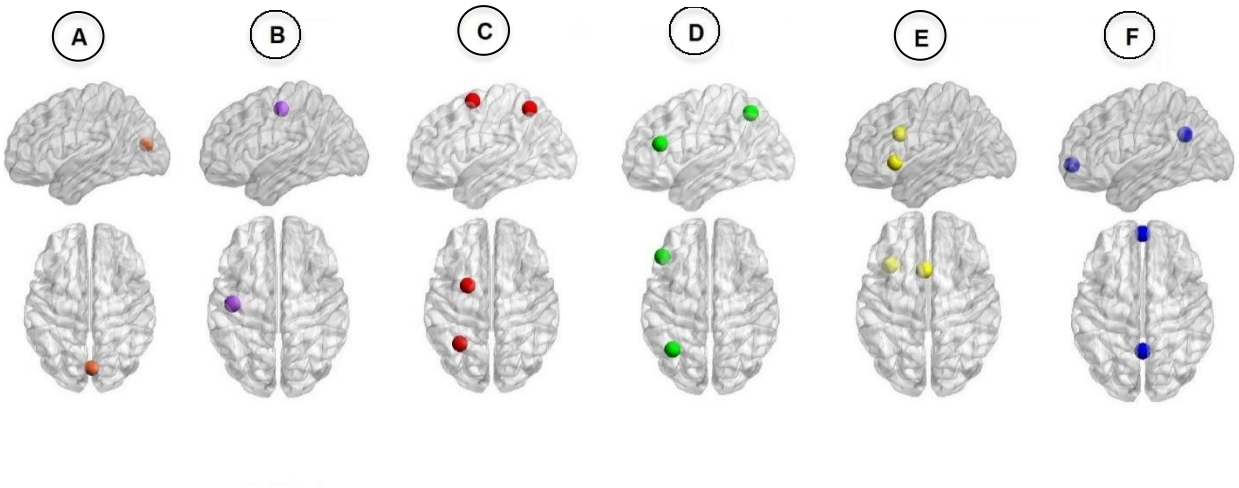

Fig. 1 *Taxonomy of the ICNs proposed by Uddin et al. (2019). Only the main nodes of each network are illustrated here by colored dots*. ***(a)*** *Occipital Network (ON),* ***(b)*** *Pericentral Network (PN),* ***(c)*** *Dorsal Frontoparietal Network (D-FPN)****,*** ***(d)*** *Lateral Frontoparietal Network (L-FPN),* ***(e)*** *Midcingulo-Insular Network (M-CIN),* ***(f)*** *Medial Frontoparietal Network (M-FPN). Adapted from Uddin et al. (2019).*

1.2.2. The stationarity debate

As mentioned before, studies of resting brains reveal the emergence of complex patterns of dynamic activity, both at a cortical and at a subcortical level. The most common procedure to measure FC is to compute the Pearson correlation between pairs of brain regions' time series (X, Y):

$$P(X,Y) = \frac{cov(X,Y)}{\sigma X \sigma Y}$$

Where $cov(X,Y)$ is the covariance between the activity of a pair of regions (X,Y) and $\sigma X \sigma Y$ is the product of the standard deviations of the activity of the two regions. This metric potentially misses relevant temporal information, given that this connectivity measure is invariant to temporal reordering of the points in the timeseries. Alternatively, to retain temporal information and investigate dFC, sliding window correlations (SWC) constitutes the easiest to implement and consequently the most employed technique. While it is still unclear if dFC is best conceptualized as continuous change or a succession of discrete non-stationary transitions, recent studies have stressed the latter perspective, identifying recurrent and discrete FC patterns, or dynamic functional states (DFSs), by applying clustering algorithms to SWC. However, it might also be the case that dynamic fluctuations in functional connectivity are due to sampling variability in FC. A common statistical procedure to rule out this possibility resides in the employment of randomization frameworks to generate null data. In this way, the statistical significance of dFC can be tested by comparing statistics from the null data with statistics from the original data, eventually rejecting the null hypothesis (i.e., dFC is to be attributed to sampling variability in static FC). The most common randomization frameworks are phase randomization (PR) and autoregressive randomization (ARR). Even with the aid of these statistical procedures, the legitimacy of dFC remains under debate. This conflict in the literature might be due to the loose usage of the term “stationarity” which, paired with the fact that models like ARR and PR rely on strict statistical definitions of stationarity, contributes to a halting progress in the study of dFC. Thus, research focused on the study of functional connectivity might benefit from a common definition for stationary and non-stationary processes, based on statistical principles. To this aim, in this thesis we provide the

definition of weak-sense stationarity (WSS) based on the work of Liégeois and colleagues (2017) as follows:

A random process X_t (such as multiple resting-state fMRI recordings) is WSS if its mean $E(X_t)$ is constant for all time t and its auto-covariance $Cov(X_n, X_m)$ depends only on the time interval $\tau = t_2 - t_1$.

Accordingly, the variance of a WSS process is constant over time. Following from this definition, one might assume that a WSS process lacks fluctuations in FC as well as DFSs. However, evidence from brain activity simulations conducted with Hidden Markov Models (HMM) suggests that stationarity does not necessarily imply the absence of FC states. This apparent paradox arises because dFC and consequent brain states exist at the level of individual realizations of a random process while considering ensemble statistics notions (i.e., statistics computed across different realizations of the same random process) such as WSS, results in averaging out these dynamics across realizations. Contributing to this ambiguity, there is the possibility that each subject might be considered as a random process of its own instead of a single realization of a common random process. This would imply that all FC measures currently employed in the literature are based on sample statistics rather than ensemble.

1.3. Main findings of Favaretto et al. 2022

A recent study by Favaretto and colleagues (2022) investigated the role of subcortical regions in shaping dynamic functional connectivity, including in their analysis both control and stroke subjects. The authors showed that cortical and subcortical regions display simultaneous FC shifts and that each DFS was associated with different patterns of cortical/subcortical interactions. In fact, alterations in cortical conditions coincided temporally with changes in subcortical interconnections. In Figure 4a of their work, Favaretto et al. (2022) present representative temporal patterns of the primary eigenvector for cortical connectivity, projected onto diverse networks, alongside the two primary components of the main eigenvector for subcortical connectivity. The synchronized reorganization of both cortical and subcortical connectivity is visually appreciable. It is worth noting that this reorganization of patterns in subcortical and cortical areas happened simultaneously, regardless of how a DFS switch was defined.

To quantify this synchronization, Favaretto et al. (2022) assessed shifts in connectivity separately for cortical and subcortical regions, measuring the differences in connectivity between consecutive sliding windows. Both cortical and subcortical connectivity shifts exhibited a distribution with a heavy tail, indicating that smaller differences were more frequent (see Fig. 4b left of Favaretto et al., 2022). Consequently, to identify connectivity shifts, they exclusively considered instances where a substantial connectivity difference occurred (i.e., “jumps”: upper 5% of the values).

Next, they examined the simultaneity of cortical and subcortical “jumps” by computing the conditioned probability of subcortical connectivity reorganization given a cortical

connectivity reorganization (see Fig. 4b right of Favaretto et al., 2022). This analysis was performed for each subject and for all networks. Across all networks, the observed probability of synchronized jumps was significantly higher than the probability predicted by independent processes, reinforcing the notion of simultaneous shifts in cortical and subcortical dynamics. It is crucial to emphasize that this analysis considered all sliding windows, not just those that defined the boundaries of DFSs. As such, the assessment of time course synchronization was not influenced by how DFSs were defined. Moreover, their analysis revealed an antagonistic interaction between two main clusters of subcortical regions object of their parcellation: basal ganglia (SC-1) and limbic nuclei (SC-2).

Additionally, Favaretto et al. (2022) captured the complexity of dFC fluctuations by means of five repeating and alternating FC patterns (i.e., DFSs). The first DFS displays a connectivity profile similar to healthy static FC, with high homotopic connectivity and modularity as well as large negative Dorsal Attention Network-Default Mode Network (DAN-DMN) connectivity. Sensorimotor attention networks (SM) are positively correlated and negatively correlated with DMN. Additionally, a positive correlation between DMN and limbic nuclei and a negative correlation between limbic and SM attention networks are present. DFS2 resembles pathological static FC after stroke, with low homotopic connectivity and modularity as well as nearly zero DAN-DMN connectivity. Moreover, this state displays a strong interaction between cognitive networks and a strong negative coupling of the Visual network (VIS) and all the others. DFS3 is characterized by high homotopic connectivity and modularity but absent strong negative DAN-DMN correlation. Also, a negative coupling between SM and cognitive clusters is appreciable. Finally, this

state exhibits an opposite connectivity pattern between SC1-SC2 and SM/DMN with respect to the first DFS. The fourth DFS shows intermediate values of FC biomarkers, a positive correlation between subcortical clusters, which are in turn negatively coupled with cortical networks. Ultimately, DFS5 has also intermediate values of homotopic and DAN-DMN connectivity as well as a very low value of modularity. This state reveals also a significant integration among almost all the considered networks (as DFS2) except for VIS and DMN.

1.4. Questions and general plan

This thesis project intends to corroborate Favaretto et al.'s findings (2022) using data from an independent and standard rs-fMRI database, made available by the Human Connectome Project (Van Essen et al., 2013). The partial replication of dynamic functional states with a different dataset could strengthen the hypothesis that dFC arises from a multistable connectivity landscape rather than being the product of sampling variability. Additionally, this work will try to assess the robustness of Favaretto et al.'s conclusions (2022) with respect to details of the methodological pipeline as well as some relevant key assumptions. Dynamic functional connectivity, in fact, can be sensitive to some aspects of the preprocessing framework. Even though a universal consensus on a single methodological pipeline might be beyond reach, the community should be aware of potential analysis pitfalls and the impact of specific data analysis choices. In particular, we will focus on the influence of different cortical and subcortical atlases as well as the individual effect of each preprocessing step adopted by Favaretto and colleagues (2022). The final goal is to further expand previous findings, trying to link dFC metrics with specific aspects of individual behavior.

2. METHODS

All the operations that constituted our analyses were conducted in the MATLAB environment and the corresponding custom algorithms are available at https://github.com/alessandronazzi/DynamicFunctionalConnectivity.

2.1. Imaging and data

2.1.1. Favaretto's dataset

All subjects included in Favaretto et al. (2022) were scanned with a 3T Siemens Tim-Trio scanner at the Washington University School of Medicine with a standard 12-channels head coil. They were divided into four experimental groups: three groups of stroke patients, depending on the time they were scanned after stroke onset (1-2 weeks, 3 and 12 months after) and one age-matched control group. Pulse sequence included a gradient-echo EPI sequence with TR=2s acquiring 32 contiguous 4 mm slices, with 4x4 mm in-plane resolution while fixating on a small white crosshair. Pre-processing included: regression of head motion, signal from ventricles and Cerebrospinal fluid, signal from white matter, global signal; temporal filtering retaining frequencies between 0.009 and 0.08 Hz; frame censoring, with framewise displacement of 0.5 mm. After all the pre-processing steps, a total of 279 subjects were considered for the analysis (114 for the 2 week's condition, 80 for the 3 month's condition, 65 for the 12 month's condition and 20 controls).

2.1.2. Human Connectome project's dataset

The HCP's dataset included 80 subjects that were scanned with a modified 3T Siemens "Connectome skyra" scanner at the Washington University, using a standard 32-channels Siemens receive head coil and a specifically designed "body" transmission coil. Pulse sequence included slice-accelerated multiband acquisition with a multiband factor of 8, spatial resolution of 2 mm isotropic voxels and TR=0.7s. All participants underwent two 15-minutes scanning sessions with opposite phase encoding directions (L/R and R/L), while fixating on a crosshair. The HCP's preprocessing pipeline is divided into two distinct protocols (Glasser et al., 2013): one applied entirely on the volume data involving temporal filtering and de-noising and the second one regarding mapping the data to cortical surfaces and sub-cortical gray-matter domains using the Connectivity Informatics Technology Initiative file format (CIFTI). One auspicious approach for removing structured artifacts involves denoising each 15-minutes rfMRI scan with the Independent Component Analysis (ICA) based tool called FSL's MELODIC. This tool, paired with the FMRIB'S ICA-based X-noisefilter, allows decomposing the data into multiple components (comprising a spatial map and a corresponding time course) and to classify them in order to subsequently regress out the confounding ones. In addition to the HCP's pipeline, we followed thoroughly the supplementary pre-processing steps adopted by Favaretto and colleagues (e.g., temporal filtering and global signal regression), in order to reduce the variability between the two analyses.

2.2. Parcellation

Both Favaretto and HCP's resulting residual time series were projected on the cortical surface of each subject divided according to the RSFC-boundary mapping developed by Gordon et al. (2016). This technique leverages abrupt transitions in resting-state functional connectivity (RSFC) to noninvasively identify the borders separating cortical areas. The original parcellation includes 333 regions, but all regions with <20 vertices (~50 mm^2) were excluded due to low signal-to-noise ratio (SNR). The remaining 324 regions were further reduced to 90 by a clustering procedure and finally grouped into 10 ICN's: Visual Network (VIS), Sensory Motor Hand-Mouth Network (SMN), Auditory Network (AUD), Control or Cingulo-Opercular Network (CON), Ventral Attention Network (VAN), Dorsal Attention Network (DAN), Fronto Parietal Network (FPN), Default Mode Network (DMN), Subcortical network (SUB) formed by 19 additional regions derived from the FreeSurfer subcortical atlas (Fischl 2012; Fischl et al., 2002), while the remaining 8 regions were not assigned to any networks (None).

2.2.1 Alternative sub-cortical parcellation

Expanding the initial analysis to aid the investigation of cortico-subcortical interactions, we decided to switch to a different parcellation of the subcortex, including both a coarse version with 8 bilateral regions and a finer grained one comprising 27 bilateral regions (see Supplementary Table 2 of Tian et al., 2020). This groundbreaking subcortical cartography was achieved by Tian and colleagues (2020), who developed gradientography: a fMRI technique similar to diffusion MRI, allowing the quantification of

subcortical connectivity gradients. This, paired with a statistical formalism to guide boundary identification, allowed them to exploit RSFC to extensively parcellate the subcortex.

2.3. Analysis' methods

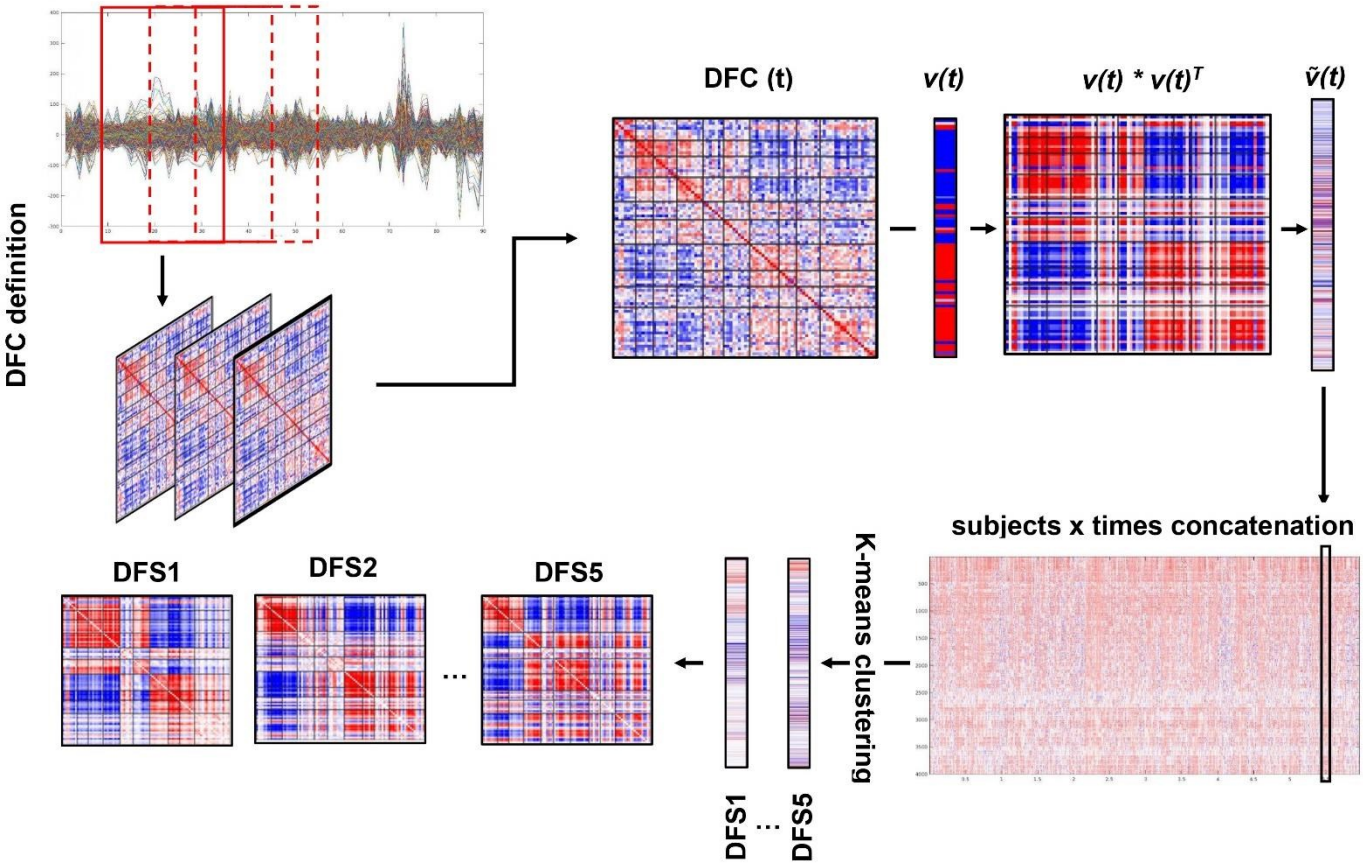

Fig. 2. *Dynamic Functional State's definition: the time course of each subject was divided into 746 time-windows of width = 28 TR (60 s) and step = 3 TR. The z-Fisher transform of the Pearson's correlation coefficient among regions was computed at each sliding window, to estimate the dynamic functional connectivity (dFC). Then, each dFC matrix was approximated by projecting on the leading eigenspace defined by the first eigenvector vi. As the eigenvectors are defined less than the sign, we avoided this issue by reconstructing the square matrix* $v_i \times v_i^T$*. After that, the upper triangular part of these dFC matrices was vectorized and concatenated across windows and subjects, in order to finally apply a time-wise K-means clustering algorithm with correlation distance to define a set of spatial DFSs.*

2.3.1. Sliding-window functional connectivity

FC dynamics were investigated through Sliding window temporal correlation (SWC), one of the most straightforward approaches for dFC analysis. Similarly to a moving average function, this technique computes a succession of pairwise Fisher z-transformed Pearson correlation matrices, relative to windows of a given width. These correlation matrices are

informative of the time-varying FC between the networks considered in the brain parcellation of choice. Importantly, to compensate for the difference in TR durations between the two datasets (i.e., Favaretto's TR=2 s and HCP's TR=0.7 s), we down-sampled HCP's timeseries to one third of the points. Then, from the down-sampled timeseries we extracted windows lasting approximately one minute (28 TRs), with a sliding step of 3 TRs (approximately 2 s). Window-length choice represents a critical point in dynamical functional connectivity analysis (Leonardi and Van De Ville, 2015). Namely, having windows shorter than the analyzed components' wavelengths might cause spurious fluctuations in dynFC. Similarly, too long windows might prevent legitimate functional fluctuations to be identified. Thus, we selected our sliding window's width on the basis of previous results, matching Favaretto et al.'s choice. Additionally, each correlation matrix was approximated by projecting it onto the corresponding eigenspace, defined by the first eigenvector $v_{i.}$ Since eigenvectors are defined less than the sign, we averted this problem by translating each eigenvector into the reconstructed square matrix $v_i \times v_i^t$, saving the vectorized upper-triangular part alone, avoiding redundancies in the data. Ultimately, all the resulting vectors were concatenated across windows, subjects, and time points.

2.3.2. Dynamic Functional States' definition

The last step for DFS's definition required the application of a time-wise K-means clustering procedure with correlation distance. K-means is a clustering technique, aiming to partition an N-dimensional population into k clusters based on a sample. Each observation belongs to the cluster with the nearest mean (e.g., cluster centroid), serving

as a prototype of the cluster, resulting, in this case, in a set of five Dynamic Functional States (all the operations descripted up to now are summarized in Fig. 2). This algorithm minimizes within-cluster variances, taking into account a range of possible distance metrics. For this analysis, we employed the correlation distance, which is defined as follows:

$$d(x,c) = 1 - \frac{(x-\vec{x})(c-\vec{c})'}{\sqrt{(x-\vec{x})(x-\vec{x})'}\sqrt{(c-\vec{c})(c-\vec{c})'}}$$

Where: x is an observation and c is a centroid. In addition, $\vec{x} = \frac{1}{p}(\sum_{j=1}^{p} x_i)\vec{1}_p$, $\vec{c} = \frac{1}{p}(\sum_{j=1}^{p} c_j)\vec{1}_p$ and $\vec{1}_p$ is a row vector of p ones. Furthermore, the optimal K value was deducted by comparing the clustering performances with different numbers of clusters (from 2 to 10), with respect to a metric for interpreting and validating the consistency within clusters of data: the Silhouette value. This parameter is a measure of the fitness of a certain data point for its cluster of belonging, compared to other clusters. This metric ranges from -1, indicating the lowest fitness and +1, indicating the highest fitness. Then, for a certain data point $i \in C_I$, where C_I is the cluster of belonging, the Silhouette value is defined as follows:

$$s(i) = \frac{b(i) - a(i)}{\max\{a(i), b(i)\}}, if\ |C_I| > 1$$

Where, $a(i)$ is the mean distance between i and all the other data points belonging to the same cluster, while $b(i)$ is the smallest mean distance between i and all the data points belonging to other clusters.

Each DFS was classified with three indices commonly employed as static FC biomarkers in stroke, namely: the average homotopic inter-hemispheric connectivity within each network (i.e., the average connectivity between homologous regions of different hemispheres forming a network); the average intra-hemispheric connectivity between Dorsal Attention network (DAN) and Default Mode Network (DMN), as a measure of network integration; and the overall Newman's modularity among cortical networks.

Additionally, the clustering procedure associated each sliding window to a specific DFS, so that for each subject we had a discrete time series $x(n)$ (with n ranging from 1 to 773), where each value represented the active Dynamic Functional State for that time window. These time courses allowed us to evaluate three dynamical measures for each state, namely: fraction time f_k, being the percentage of times during which a state is active:

$$f_k = \frac{\#(x(n) = k)}{773}, k = 1, \dots, K$$

where $\#(a)$ stands for the number of occurrences of the condition a. The dwell time l_k, being the average length of periods in which each state remains continuously active:

$$l(k) = \frac{1}{|L_k|} \sum_{i=1}^{|L_k|} L_k[i]$$

where L_k is the set having cardinality $|L_k|$, with each element $L_k[i]$ representing the length of a period of continuous activity of state k. The transition probability $DFS_i > DFS_j$, from $DFSi$ to $DFSj$, where:

$$DFSi > j = \frac{\#(x(n) = i \wedge x(n+1) = j)}{\#(x(n) \neq x(n+1))}$$

being the ratio between the number of jumps from $DFSi$ to $DFSj$ over the total amount of jumps.

2.4. Methodological investigations

2.4.1. Phase randomization

Phase randomization (PR) is a common framework for generating null data extensively employed in physics. Recently, it has also been applied to fMRI data for studying dynamic FC (Allen et al., 2014). The PR procedure generates null data with the same correlation properties as the original signal. Specifically, it performs a Discrete Fourier Transform (DFT) of the original time series, adding a uniformly distributed random phase to each frequency, and then performing the inverse DFT to create surrogate data. Crucially, the random phases are created individually for each frequency, yet remaining consistent across various regions of the brain.

2.4.2. Normalized mutual information

Mutual information is a concept from information theory that measures the amount of information that two random variables share. It serves as a metric for assessing the level of interdependence or correlation between these variables. In simpler terms, mutual information tells us how much knowing the value of one variable can help us predict the value of another variable. Thus, the mutual information $I(X;Y)$ between two random variables X and Y can be denoted as:

$$I(X;Y) = H(X) + H(Y) - H(X,Y)$$

where $H(X)$ is the entropy of a random variable X, measuring its uncertainty and $H(X,Y)$ is the joint entropy of X and Y. A common alternative version of this measure is normalized

mutual information (NMI), that can be employed for determining the quality of a clustering by comparing the level of agreement between two different partitions (Romano et al., 2014). The interpretation of mutual information is that a value closer to zero indicates less association between two variables while a value farther away from zero indicates more association between two variables. NMI can be computed as follows:

$$nmi = I(X;Y)H(X)H(Y)$$

2.5. The impact of dFC on behavior

2.5.1. Individual measures

For the investigation regarding the behavioral implications of dFC we selected indices and test performances included in the Human Connectome Project database, relative to the 80 subject that were part of the initial analyses. The measures that we extracted belonged to two major domains: alertness and cognition (WU-Minn HCP, 2017), and were culled in that they covered aspects of cognitive capabilities that support the anticipatory and predictive effort of our brain.

The level of alertness, as a state of active attention marked by heightened sensory perception, was assessed by the Mini-Mental State Examination (MMSE, Folstein et al., 1975) and the Pittsburgh Sleep Quality Index (PSQI, Buysse et al., 1989). The MMSE is a 30-point questionnaire extensively employed to measure cognitive impairment that was administered, within the HCP consortium's framework, as a broad measure of cognitive status. The participants scoring below 27 were excluded following the work of Crum and colleagues (1993). Administering the MMSE takes between 5 and 10 minutes and examines functions including registration, attention and calculation, recall, language, ability to follow simple commands and orientation. The PSQI is a self-report questionnaire, consisting of 19 individual items grouped in 7 components that result in one global score assessing sleep quality. This test takes between 5 and 10 minutes to complete and has to be repeated every day for a month.

Cognition was assessed through fluid intelligence, processing speed and sustained attention metrics. Fluid intelligence is strongly related to specific functional performances

and to variations in neuronal structure in humans (Duncan et al. 2000; Duncan 2003; Duncan 2005). Levels of fluid intelligence are usually measured by Raven's Progressive Matrices (Prabhakaran et al. 1997). In the HCP database they employed Form A of an abbreviated version of this test developed by Bilker and colleagues (PMAT24, 2012). The task has 27 items (24 standard and 3 bonus) of increasing difficulty. Participants must pick the response that best fits the missing square on a pattern made up of 2x2, 3x3 or 1x5 arrangements of squares, among five possible responses. Processing speed (PS), defined as the amount of time required to complete a task, is believed to form the basis for other cognitive functions such as memory and working memory (Baudouin et al., 2009; Chiaravalloti et al., 2003), attention (Mayes and Calhoun, 2007) and executive functioning (Baudouin et al., 2009). PS was assessed through the Pattern Comparison Processing Speed Test (PCPST) of the National Institutions of Health Toolbox for the Assessment of Neurological and Behavioral Function (NIHTB, Carlozzi et al., 2015). In this test participants have to determine whether two visual patterns are identical or not by pressing a "yes" or "no" button. Non-identical patterns vary on one of three dimensions: color, adding/taking something away, or one versus many (only for subjects of 3 to 15 years old. Scores are assigned as a consequence of the number of correct items (maximum 130 points) presented over a 90 s period of time. Finally, sustained attention (SA), which enables individuals to maintain attentional focus on relevant stimuli over an extended period of time, is among the key executive functions and a dominant component of attention (Sarter et al., 2001). SA's assessment was conducted through the administration of the Number/Letter version of the Short Penn Continuous Performance Test (SCPT, Gur, 2010). Participants are presented with vertical and horizontal red lines, flashing on

the computer screen. In one of the two blocks they have to press the spacebar whenever the lines form a number, while in the other block they must press the spacebar when the lines form a letter. The lines are displayed for 300 ms followed by a 700 ms ITI. Each block contains 90 stimuli which are displayed for 300 ms followed by an interval of 700 ms, lasting a total of 1.5 minutes.

2.5.2. Statistical analysis

We assessed the impact of variability in dFC patterns via a Generalized Linear Model (GLM) which included fraction and dwell times as alternative predictors and the performance of the tests presented above as different dependent variables. GLM are a special class of non-linear regression models, using linear methods, which allows to describe non-linear relationships between a dependent variable and one or more predictive terms. The distinctive features of linear models are generalized in GLM as follows:

1. For each set of values of the predictors X, the dependent variable can present different distributions, namely: normal, binomial, Poisson, gamma, or inverse Gaussian, with parameters including the mean μ.
2. A coefficient vector b defining a linear combination of the predictors Xb.
3. A link function f defining the model as $f(\mu) = Xb$.

3. RESULTS I – Replication

3.1. Replication with the same parameters

The core of this work is devoted to a replication of the main findings of Favaretto et al. (2022) with an independent dataset, provided by the HCP consortium. The main motivation behind this effort is to test the validity and generalizability of the main findings of the previous study.

In a first analysis, we tried to replicate results by remaining as close as possible to the analysis pipeline used by Favaretto et al. (2022). Apart from minor details in the preprocessing, our pipeline thus matched analysis choices made by Favaretto et al. (2022). This includes using the same atlas (reduced Gordon-Laumann atlas + 19 subcortical regions), the same metric (correlation distance) in FC space, the same number of clusters (K=5), the same temporal resolution (~2s), and keeping the same attitude towards the global signal (that was regressed out). In later analyses, we shall discuss at length the possible effects of each of these specific choices, by varying one or more of these parameters.

Among the main results of Favaretto et al. (2022), we focused on DFSs' definition and cortico-subcortical activity coupling, neglecting stroke-related analysis (Given the absence of stroke patients in the HCP's dataset employed for this study).

3.1.1. Dynamic Functional State's comparison

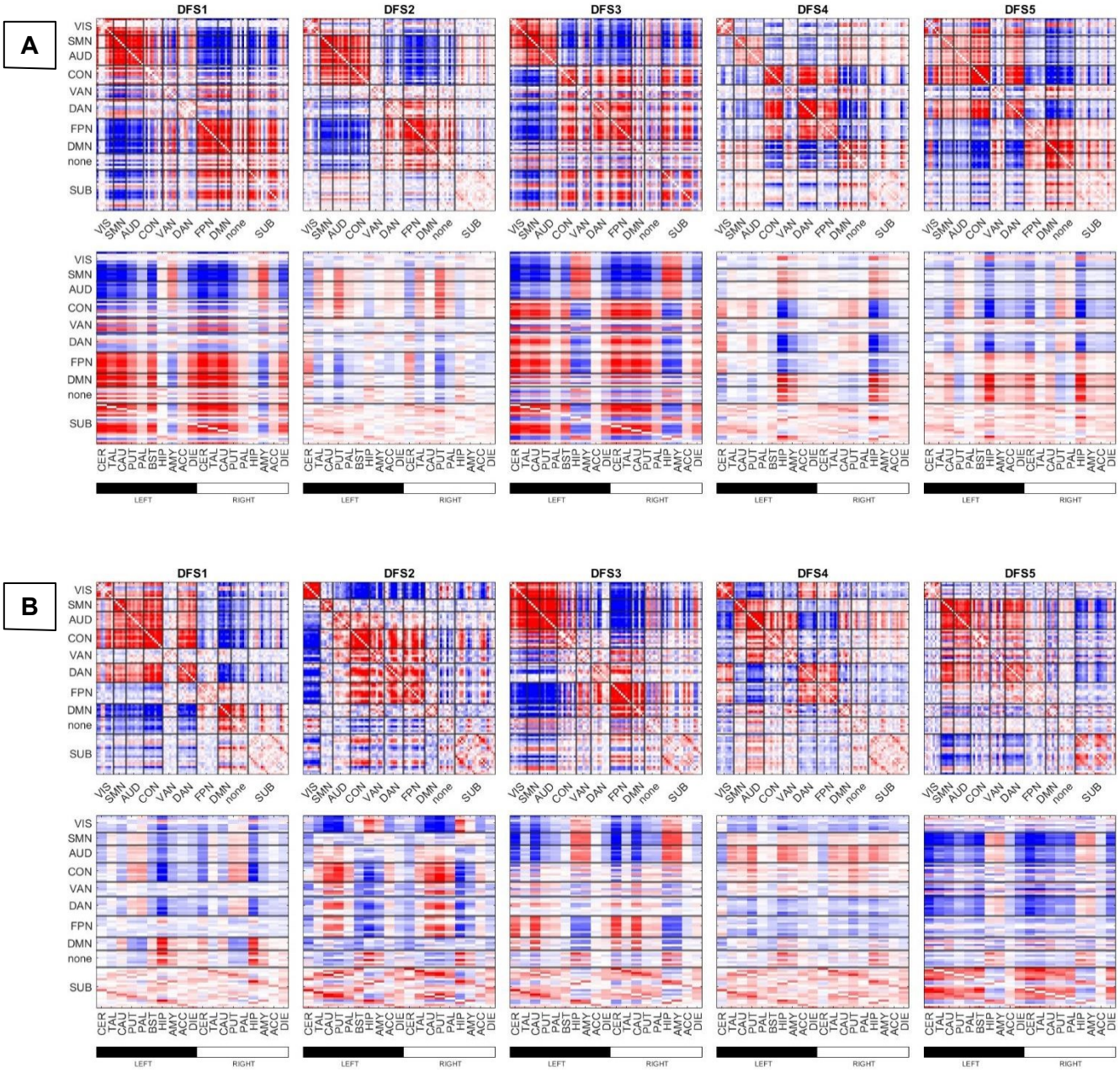

Fig. 3. (a) *We show the cluster centroids of the K=5 dynamic functional states (DFS) found in the HCP data set. Each centroid v is shown in matrix form, by plotting the matrix v x* v^T*.* ***(b)*** *As in* ***(a)****, but for the Washington dataset. The bottom row of* ***(a)*** *and* ***(b)*** *is a zoom in of the cortico-subcortical interaction.*

In Fig. 3a we plot the K=5 states found in the HCP data set (“new data set”), along with their counterparts in the Washington dataset (“old dataset”) (Fig. 3b). We registered a partial qualitative overlap between Favaretto’s and our results. In what follows, we will qualitatively compare the new and old states, and possibly match them, substantiating our discussion with quantitative evidence from a confusion matrix showing the correlation values for all the possible combinations of old and new states (Fig. 4).

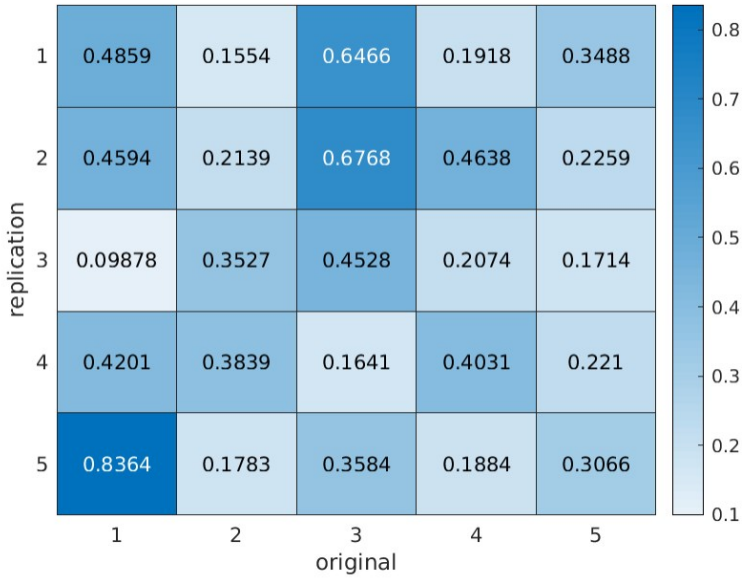

Fig. 4. *A confusion matrix with the Pearson correlation values for each couple of DFSs between Favaretto’s (x axis) and our replication study (y axis).*

In detail, we can appreciate that the “old” DSF1 is approximately reproduced by the “new” DFS5, with a correlation of 0.84. More specifically, they both display high DAN/DMN segregation, relatively high homotopic connectivity and similar levels of modularity (Fig. 5). Additionally, they are characterized by positive limbic-DMN connectivity and negative limbic-DAN connectivity. The “old” DFS3 is partially reproduced by the “new” DFS1 and DFS2 (0.65 and 0.68 of correlation respectively), with significant DAN/DMN integration,

high homotopic connectivity, high modularity, negative limbic/DMN connectivity (especially “new” DFS1) and a negative coupling between cognitive clusters and sensorimotor clusters. The “old” DFS4 instead, despite a general low correlation value (i.e., 0.46), resembles the “new” DFS2 with respect to the cortico-subcortical interaction. In fact, they both show a generally weak cortico-subcortical connectivity. However, the “old” DSF2 and DFS5 could not be associated with any of the new DFSs. Regarding the former, it might be a consequence of the presence of stroke patients in the Washington dataset, potentially biassing results by including pathological features of post-stroke connectivity.

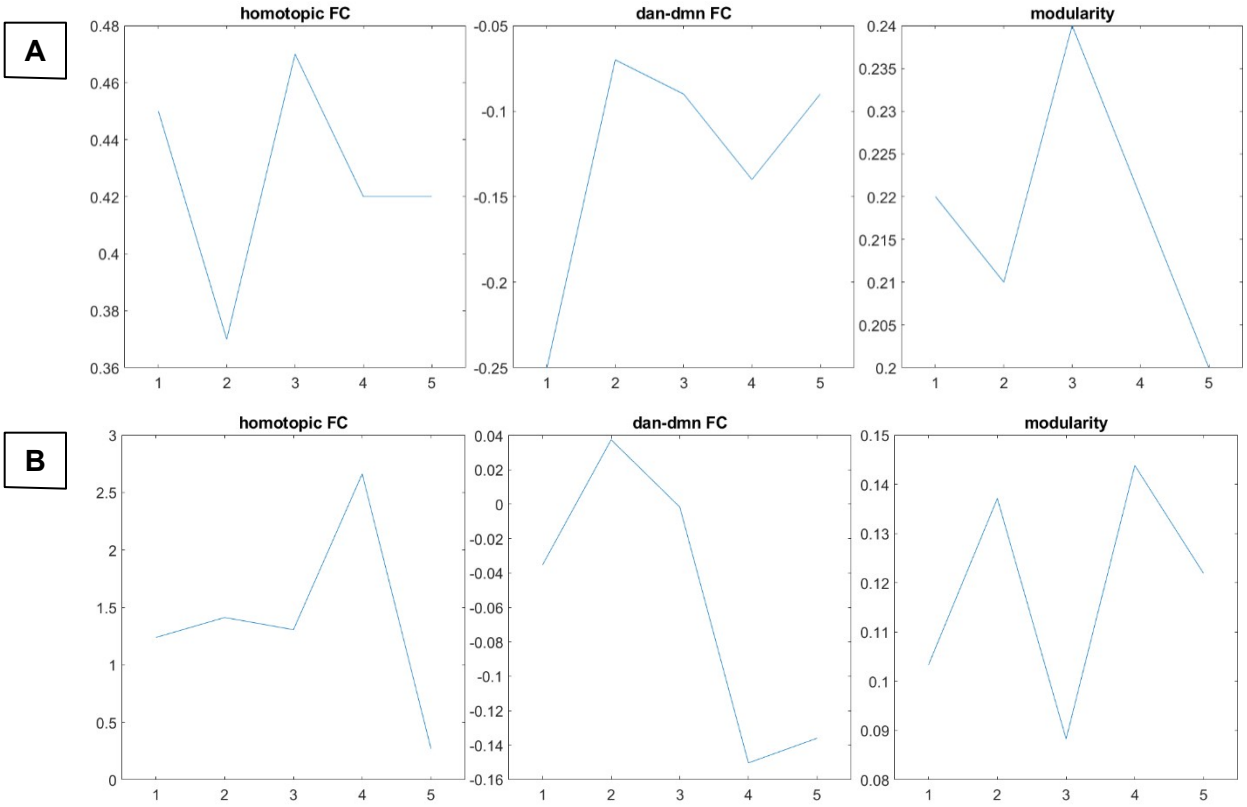

Fig. 5. *We plot three common FC connectivity biomarkers in stroke for both Favaretto’s* ***(a)*** *and our dataset* ***(b),*** *namely the average homotopic inter-hemispheric connectivity within each network; the average intra-hemispheric connectivity between Dorsal Attention network (DAN) and Default Mode Network (DMN); and the overall Newman’s modularity among cortical networks.*

3.1.2. Cortico-subcortical activity synchronization

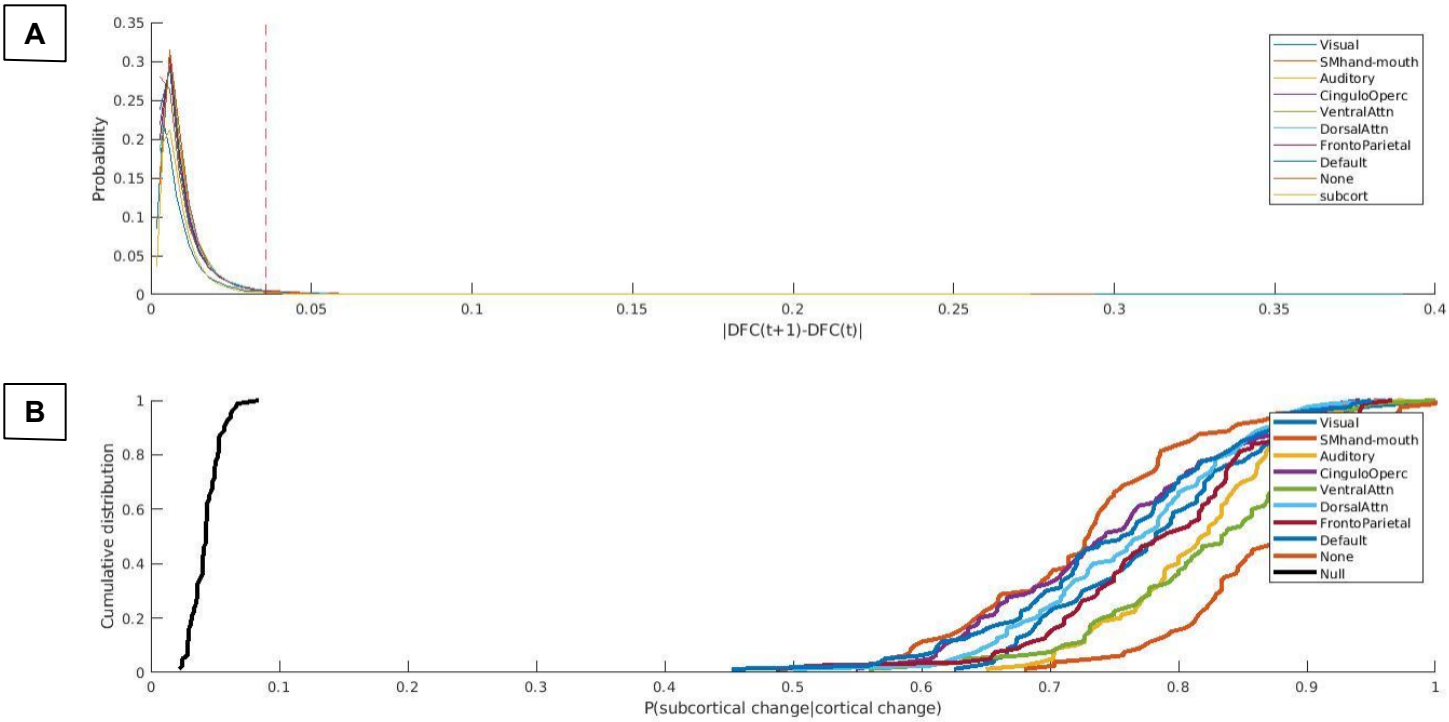

Fig. 6. (a) *Probability distribution of the absolute values of connectivity differences between consecutive sliding windows. Each line represents a different network.* ***(b)*** *Cumulative density function of the conditioned probability of subcortical connectivity reorganization, given a cortical connectivity reorganization. Each colored line relates to a different cortical network. The black line shows the cumulative density function under the null hypothesis of independence between cortical and subcortical changes.*

Importantly, even in the absence of an exhaustive correspondence between the DFSs of the two studies, we confirmed the existence of simultaneous connectivity reorganization between cortical and subcortical networks. In fact, connectivity shifts happened jointly for cortical and subcortical regions. In Fig. 6a is displayed the distribution of the differences between FC patterns in consecutive sliding windows, both at the cortical and subcortical level. From the heavy tail of this distribution, we can conclude that low differences in FC patterns are far more frequent. For this reason, in line with Favaretto et al. (2022), we labelled connectivity reorganizations as shifts (or “jumps”) only when the difference in

connectivity was above the 95th percentile (dotted line in Fig. 6a). Congruently with what was found by Favaretto et al. (2022), we confirmed that subcortical jumps were much more synchronized with cortical jumps than randomly expected (as represented by a null model of independent subcortical and cortical jumps, black line in Fig. 6b). In Fig. 6b in fact, we plot the cumulative density function of the conditioned probability $P(subcortical\ jump|cortical\ jump)$ for each cortical network, which is significantly larger than the probability under the null hypothesis of independence. Additionally, Favaretto and colleagues (2022) also showed an invariance of this cortico-subcortical dynamics' coordination with respect to the specific subcortical parcellation employed.

3.1.3. Dynamic Functional State's metrics comparison

In Fig. 7a we show the main cluster metrics (fraction times, dwell times) associated with the K=5 DFSs found in the HCP data set. Regarding fraction times, we can notice that the states are generally equally distributed over the time series (~20%) apart from DFS2 which is slightly underrepresented (Fig. 7a). This pattern resembles what emerged in Favaretto et al. (2022), with four states equally distributed and one outlier (Fig. 7b). In our analysis the state that was less present in the time series was the one displaying under average levels of cortico-subcortical connectivity. Considering dwell times, we registered a general alignment to what obtained by Favaretto et al. (2022), with average dwell times falling between 10 and 15 TR (see Fig. 7a). Here, we also show one example of average connectivity during time (70TR i.e., ~2 minutes) for cortical and subcortical networks (top

and bottom of Fig. 8 respectively) and an alternative visualization of the cortico-subcortical interaction, captured in brain surface/volume maps (Fig. 9).

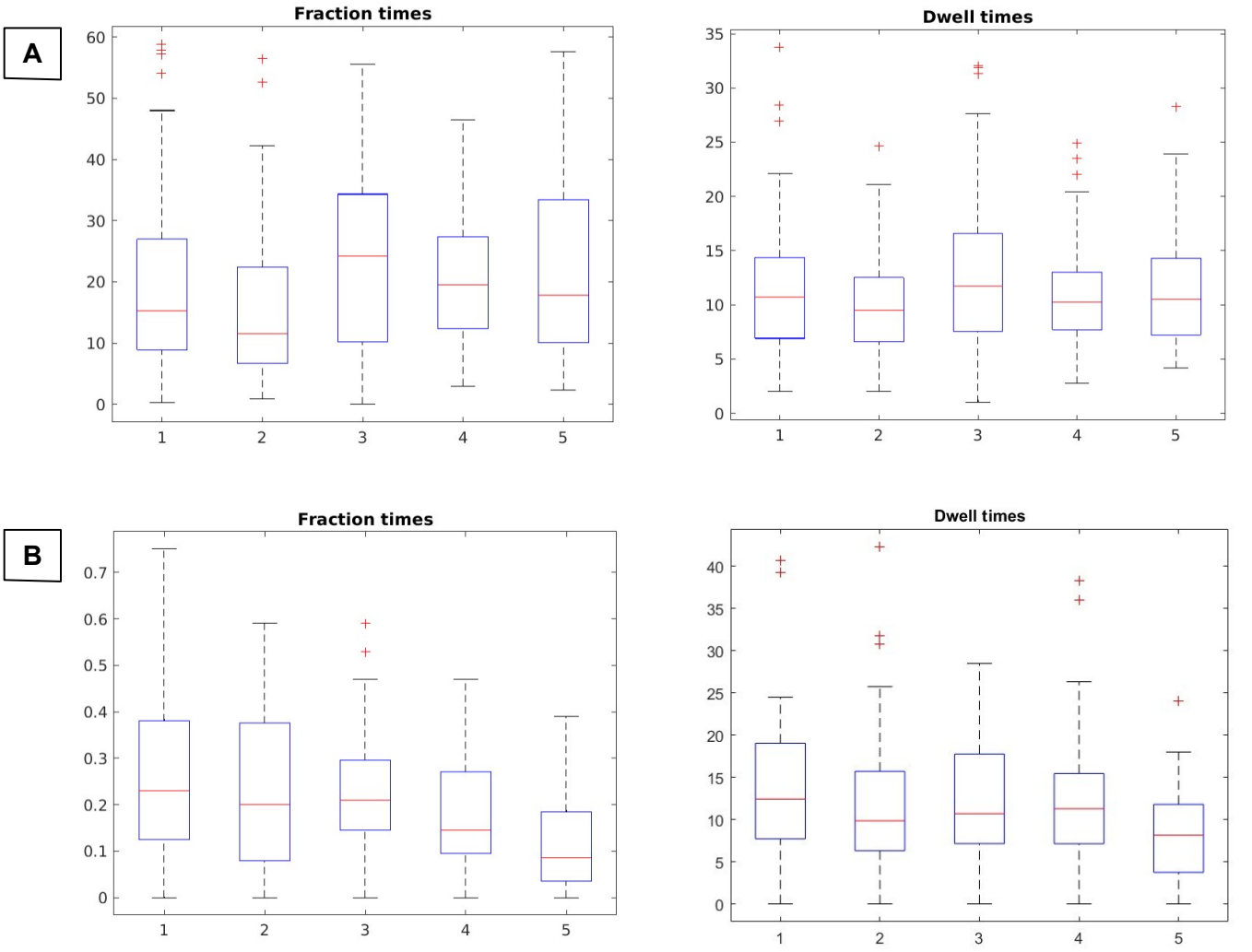

Fig. 7. *We plot the distribution of fraction and dwell times for the K=5 states regarding both our study* ***(a)*** *and Favaretto's.* ***(b)*** *Each metric was averaged within subjects and then plotted across subjects, resulting in box plots that display the median values (red lines), the interquartile range (upper and lower margins of the box representing the third and the first quartile respectively), the minimum and maximum values (whiskers) and eventual outliers (red crosses).*

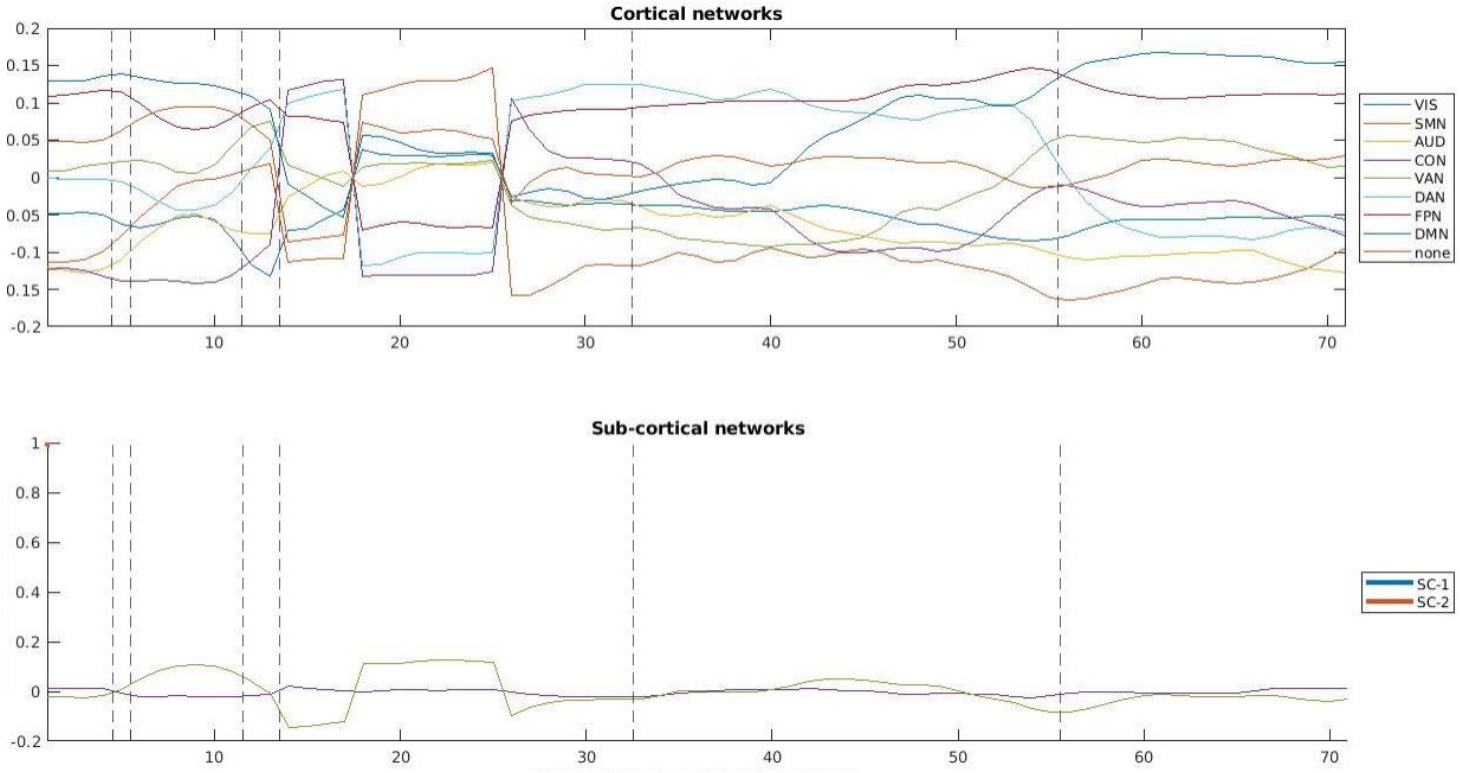

Fig. 8. *One example of average connectivity during time for cortical networks (top) and subcortical clusters (bottom). The vertical dashed lines mark the switching time points between DFSs.*

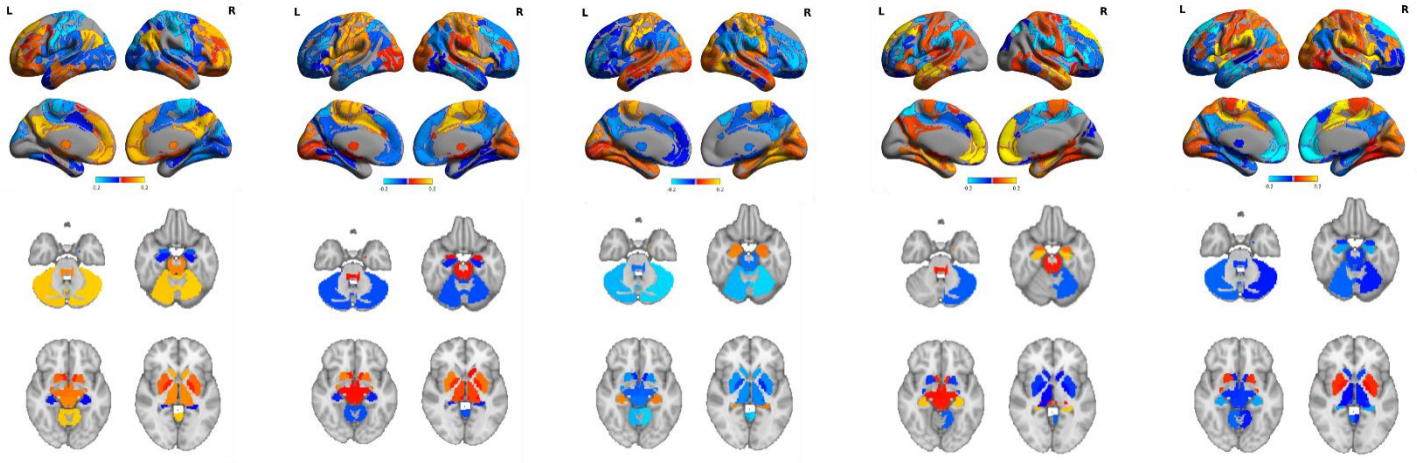

Fig. 9. *Surface and volume projection of the first eigenvector of each DFSs. Cortical regions are shown in surface (top), while subcortical regions in volume (bottom).*

3.2. Selection of the optimal number of clusters

We then proceeded to investigate the effect of tweaking different parameters, originally aligned with Favaretto et al. (2022), assessing the impact of these changes on the connectivity patterns. Specifically, we started by redoing the clustering for different values of K (from 2 to 6), registering the associated Silhouette values. According to this metric, the optimal number of clusters for our dataset was 2 (Fig. 10), which was not in line with our work of reference (Favaretto et al., 2022). However, this outcome is consistent with what we show in Fig. 12, where the continuity between the groups of data points likely reflects an excessive division in clusters. The two states emerging with K=2 correspond with DFS3 and DFS5 respectively (K=5). Interestingly, these two states capture the competitive relationship between basal ganglia/thalamus and limbic nuclei, with DFS5 showing a positive correlation between DMN and limbic nuclei and DFS3 showing the opposite FC pattern. Additionally, DFS5 maintains a FC profile similar to healthy static FC. As appreciable in Fig. 11, increasing the number of clusters led to the inclusion of new states without altering the original set present with K=3 and, predictably, to an increase in the NMI score (Table I).

Table I. *Normalized Mutual Information scores corresponding to different values of K.*

	K=2	**K=3**	**K=4**	**K=6**
Normalized Mutual Information	0.32	0.47	0.5	0.68

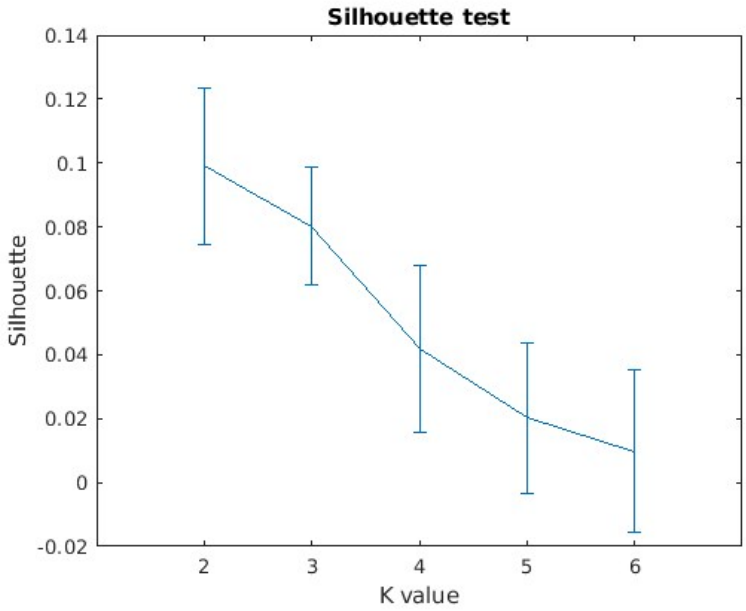

Fig. 10. *Silhouette values corresponding to different number of clusters (K value).*

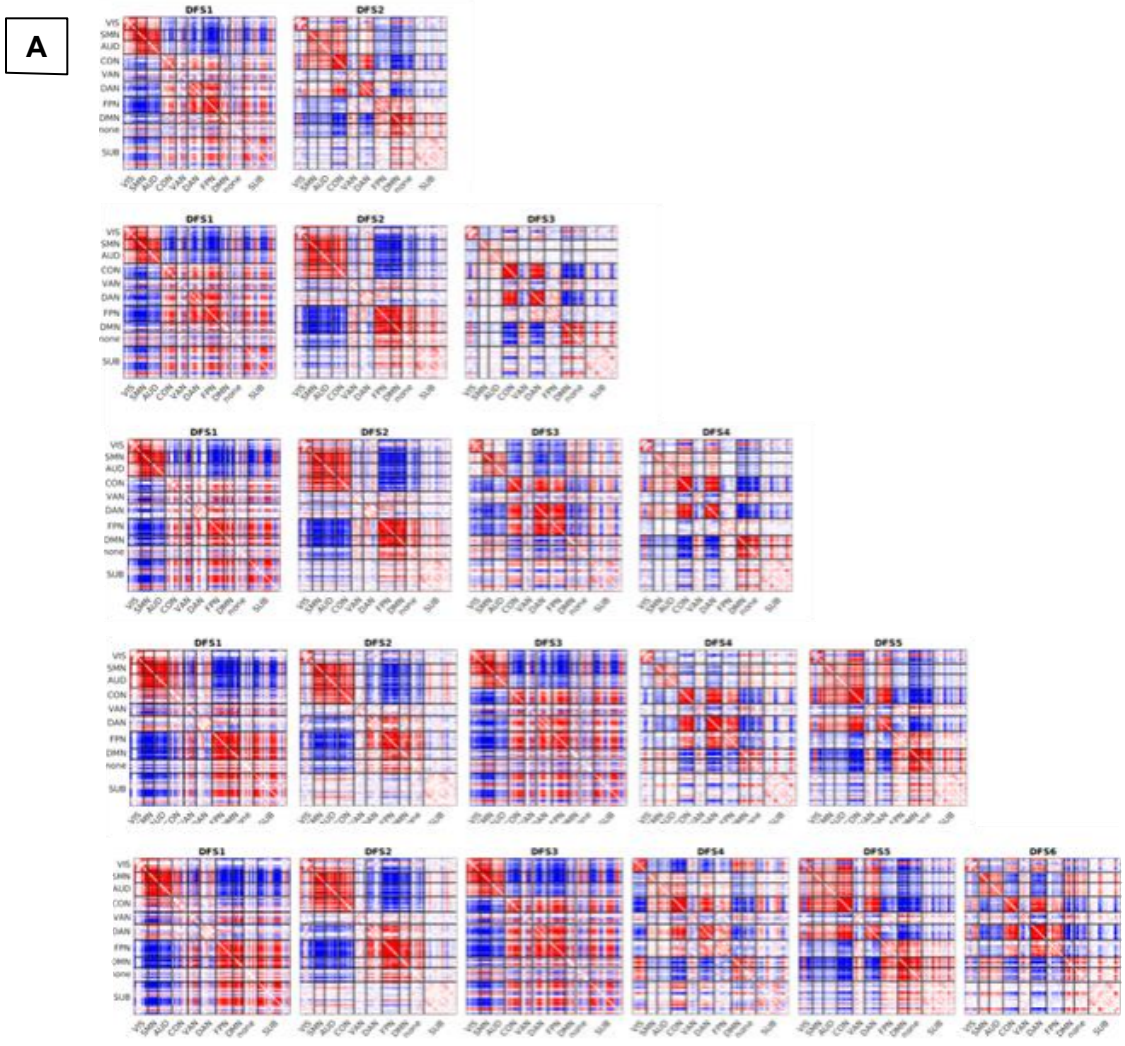

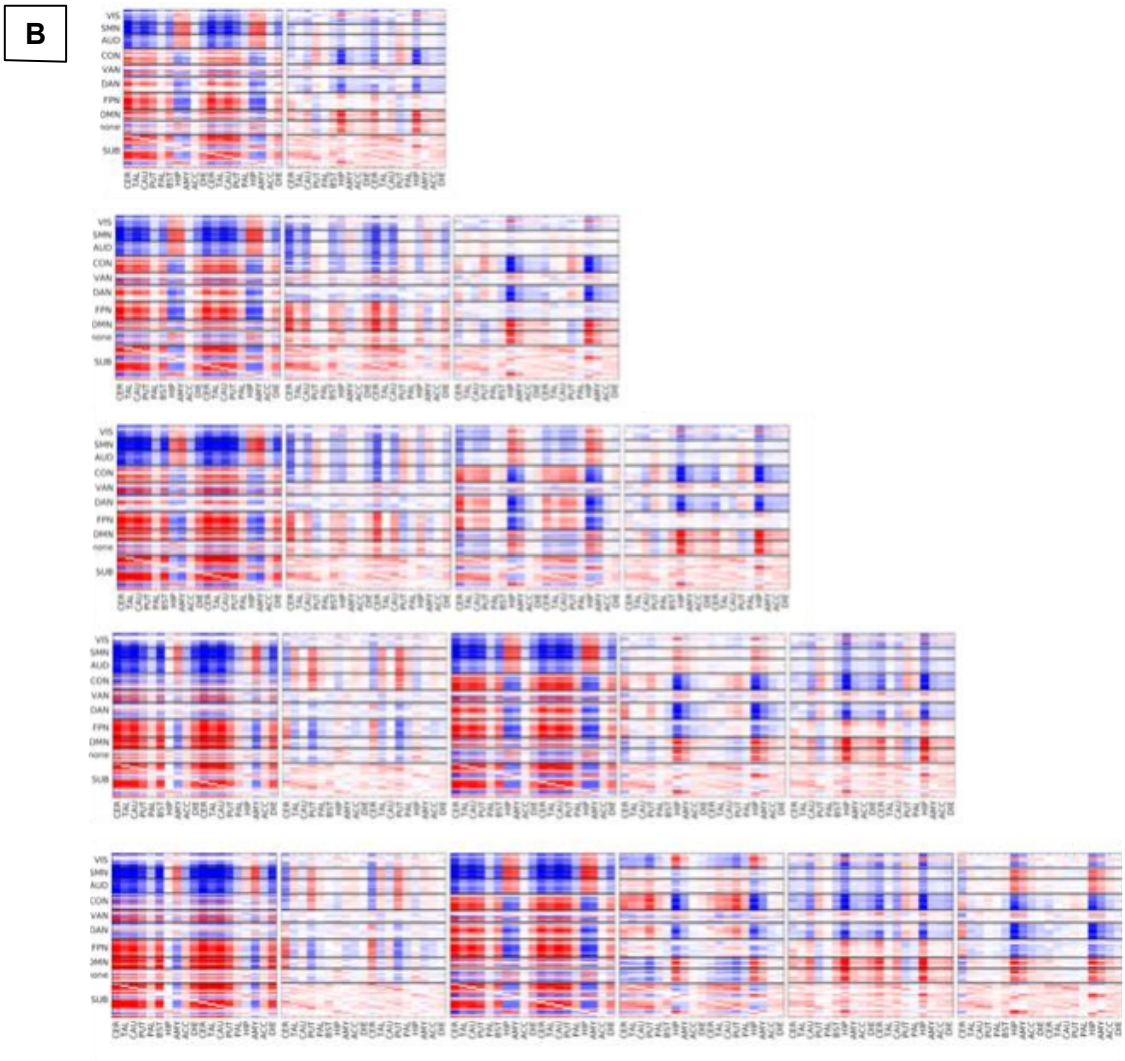

Fig. 11. *Dynamic Functional States for each value of K displayed entirely* ***(a)*** *and with a zoom in of the cortico-subcortical interaction* ***(b)****.*

To further investigate the cluster division, we applied Principal Component Analysis (i.e., a dimensionality reduction technique that linearly transforms the data into a new coordinate system, capturing the variation in the data with fewer dimensions) to the eigen decomposition of the subjects' time series and plotted the first two components (Fig. 12). This allowed us to project our dataset into a bidimensional space, in order to conveniently visualize the subdivision in clusters. Importantly, a sharp division in clusters

is missing, resulting in partial overlap between the groups, in agreement with what we observed with the Silhouette test.

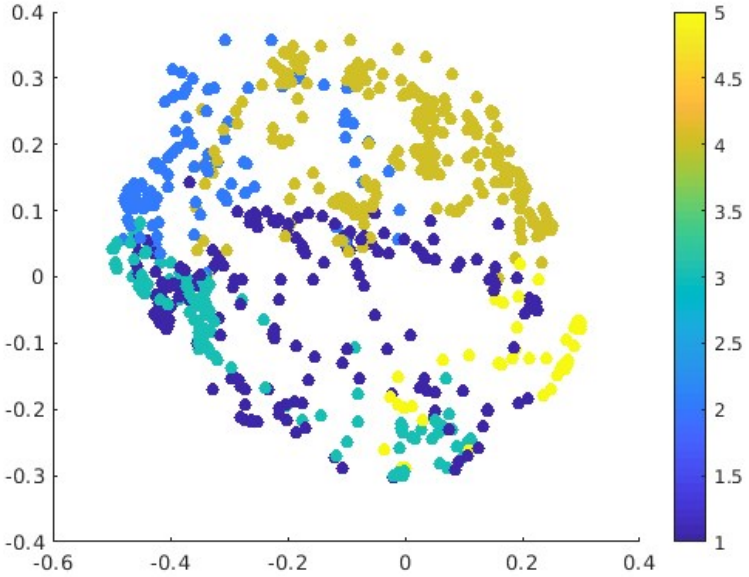

Fig. 12. *First 2 components of a PCA applied to the eigen decomposition of the first subject's time-series. The first and the second principal components are displayed on the x and the y axis respectively.*

3.3. Additional investigations

In this phase, we also explored the role of the distance metric employed in the K-means clustering. In particular, we switched from correlation to squared Euclidean distance, where each centroid is the mean of the points in that cluster, defined as follows:

$$d(x, c) = (x - c)(x - c)'$$

Finally, we checked different combinations of the preprocessing steps to rule out the effect of each one of them, particularly addressing subsampling of the timepoints and global signal regression. The sets of DFSs resulting from these exploratory analyses are grouped in Fig. 14, with a confusion matrix for each condition (Fig. 13) and corresponding NMI values (Table II).

Table II. *Normalized Mutual Information scores corresponding to different additional analyses.*

	All points	**No GSR**	**Euclidean distance**
Normalized Mutual Information	0.45	0.07	0.62

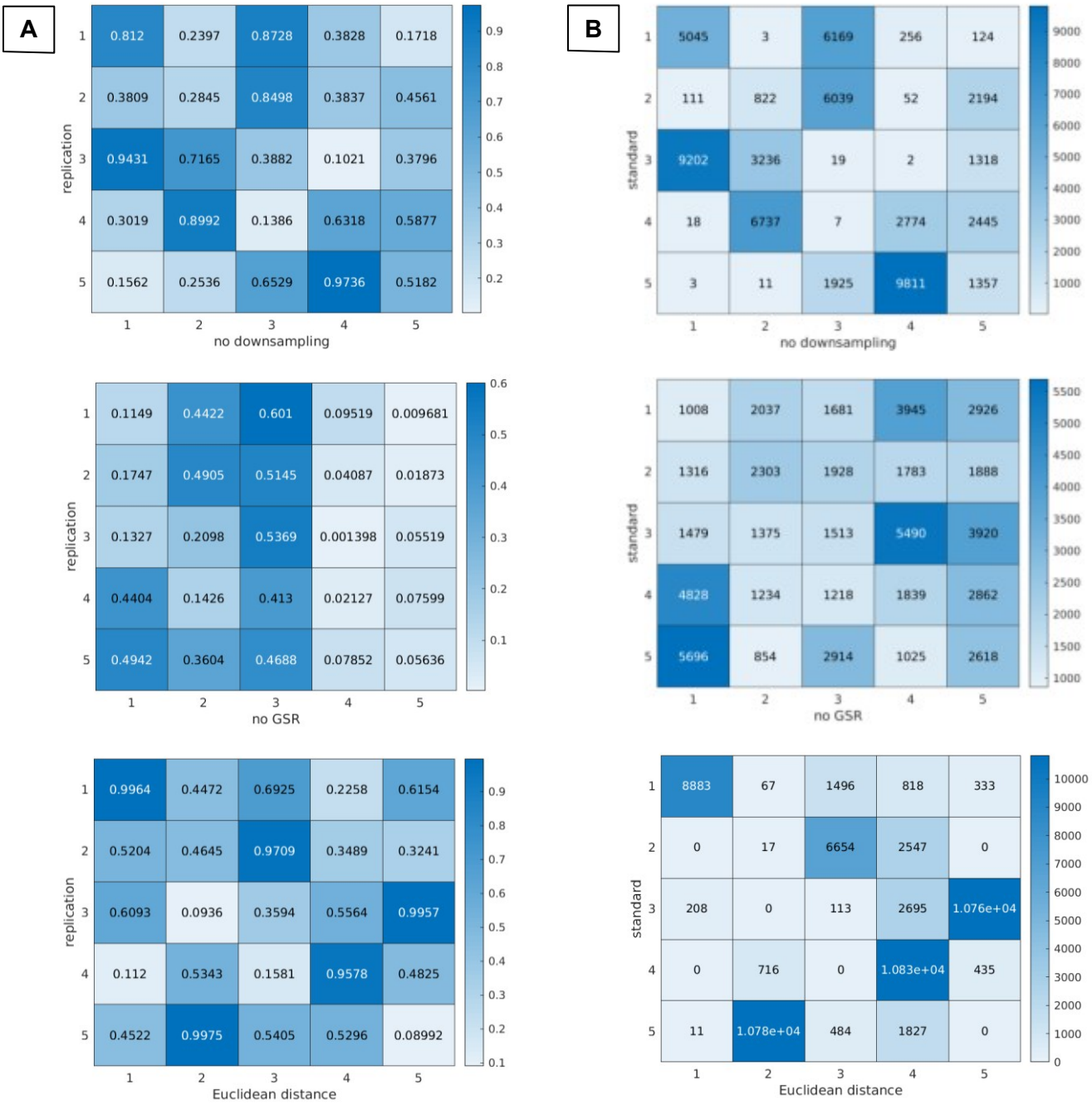

Fig. 13. *Confusion matrices showing correlation values between the centroids* ***(a)*** *and cluster's assignation for each condition* ***(b)****. Replication stands for the results obtained with the exact same parameters as Favaretto et al. (2022).*

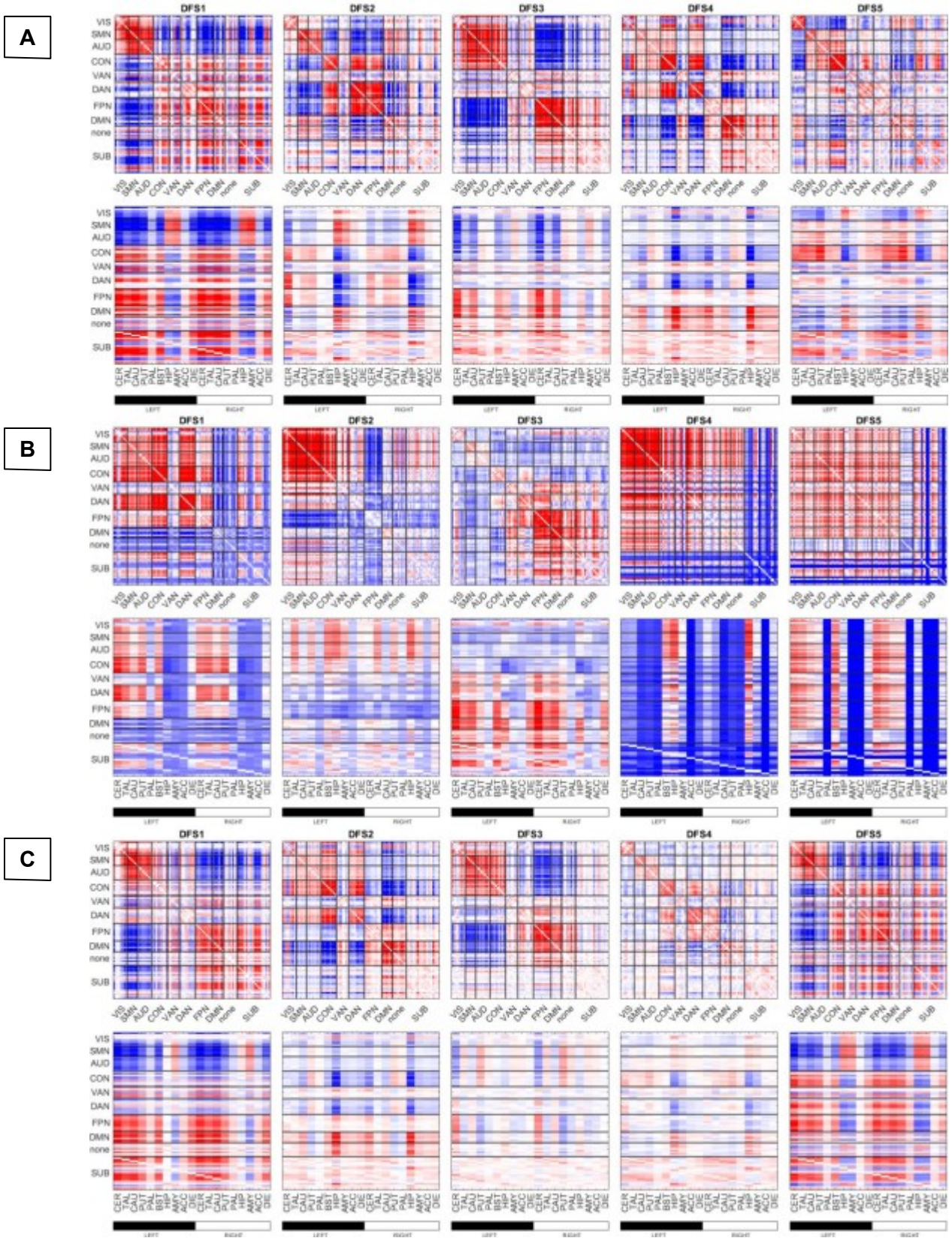

Fig. 14. *Dynamic Functional States corresponding to each condition of the additional analyses, namely: without down-sampling* ***(a)****, without GSR* ***(b)*** *and with Euclidean distance as parameter for the K-means clustering* ***(c)****.*

3.4. Summary

This replication study allowed us to confirm some of the FC patterns found by Favaretto and colleagues (2022) in a broader and independent database (i.e., HCP), as well as the simultaneous connectivity reorganization happening between cortical and subcortical networks. Specifically, we registered a significant amount of congruence between the two sets of Dynamic Functional States, with three DFSs having a convincing counterpart in the new database (i.e., “old” DFS1 to “new” DFS5, “old” DFS3 to “new” DFS1/2 and “old” DFS4 to “new” DFS2).

We then proceeded to test the robustness of these results with respect to the specifics of the methodological pipeline adopted by Favaretto and colleagues (2022), by altering parameters regarding DFSs definition and preprocessing. As depicted in the confusion matrices included in Fig. 13, Global Signal Regression had the highest impact on both cluster assignment and centroids, exhibiting the lowest NMI value (i.e., 0.07). Temporal down sampling however had a strong impact on cluster assignment without altering the DFS’s configuration. Finally, the metric of choice for the clustering procedure seemed to have virtually no effect on FC patterns, resulting in a solid NMI score (i.e., 0.62).

By plotting the first 2 components of a PCA applied to the eigen decomposition of the first subject’s time-series, we were able to project our dataset into a bidimensional space, visualizing the subdivision in clusters. In Fig. 12 we can easily appreciate the lack of well-isolated clusters derived from our analysis. This ambiguous cluster division probably impacted the additional analysis conducted with different preprocessing steps, with difficult cluster assignment and consequent low NMI scores.

As emerged from our K selection procedure, we can assume that the variability in dFC of our dataset would be best captured with a lower number of clusters (i.e., K=2). Interestingly, the two most robust states of our replication study (i.e., DFS3-5), appearing also for K=2, preserve the alternating connectivity pattern between the hippocampus and DMN/primary networks (VIS/SMN/AUD) emerged also in Favaretto et al. (2022), although to a lower extent.

4. RESULTS II - The impact of different parcellations

In this section, we will present what we observed maintaining the same preprocessing steps of the replication study but with different brain parcellations. Specifically, we tested an alternative cortical atlas based on the work by Schaefer and colleagues (2018), and an alternative subcortical parcellation (Tian et al., 2020). Testing dynamic functional connectivity results with different brain parcellations is a critical step in neuroimaging research. It helps to assess the robustness and generalizability of the findings while avoiding potential biases introduced by the choice of parcellation. Different brain parcellations, in fact, divide the brain into different regions or nodes. These regions may vary in terms of size, shape, and anatomical or functional homogeneity. Testing with different parcellations helps to determine how sensitive dFC results are to the choice of parcellation, allowing us to assess if the observed dFC patterns are heavily influenced by the specific regions used.

4.1. Schaefer's cortical atlas

The Schaefer's cortical atlas provides parcellations at multiple levels of granularity, ranging from relatively coarse divisions of the brain to finer-grained ones. The one employed for this analysis comprised 100 cortical regions, grouped into 7 networks: Visual network (VIS), Somatomotor network (SMN), Dorsal and Ventral attention network (DAN/VAN), Limbic network (LIM), Control or Cingulo-Opercular network (CON) and Default Mode network (DMN).

4.1.1. Dynamic Functional State's comparison

Surprisingly, switching to a different cortical atlas altered significantly the qualitative aspect of the states (Fig. 15). Even conducting a more rigorous comparison, the two partitions of the dataset appear to be at odds, with an NMI score of 0.08. To test the level of agreement of the two parcellations, we computed a confusion matrix showing the overlap of the cluster assignments in the two parcellations. Interestingly, we can see that points assigned to a specific cluster in the Gordon Laumann parcellation are almost consistently assigned to the corresponding cluster in the Schaefer's parcellation (Fig. 16), with only standard's DFS2 difficultly converging on a single centroid of the alternative parcellation.

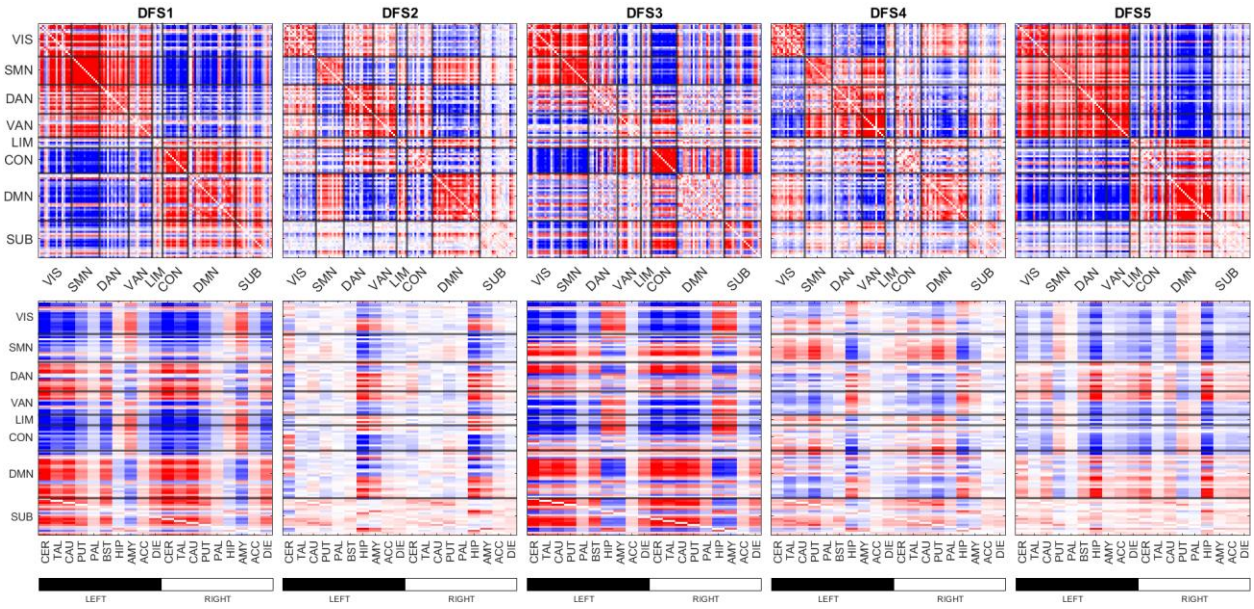

Fig. 15. *Dynamic Functional States obtained with the cortical atlas developed by Schaefer et al. (2018).*

Additionally, if we consider the two most robust states obtained with this parcellation by reducing the number of clusters (i.e., DFS3 and DFS5 are preserved for K=2) (Fig. 17), we can conclude that the alternating connectivity pattern observed before between limbic regions (i.e., hippocampus and amygdala) and DMN/primary networks (VIS/SMN/AUD), appears to be invariant to the cortical parcellation of choice.

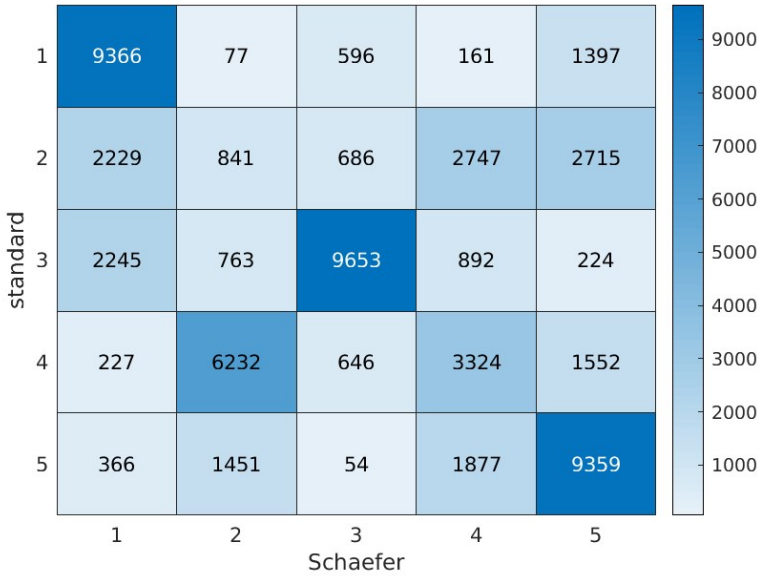

Fig. 16. *A confusion matrix with cluster's assignation between Gordon Laumann's atlas (y axis) and Schaefer's atlas (x axis).*

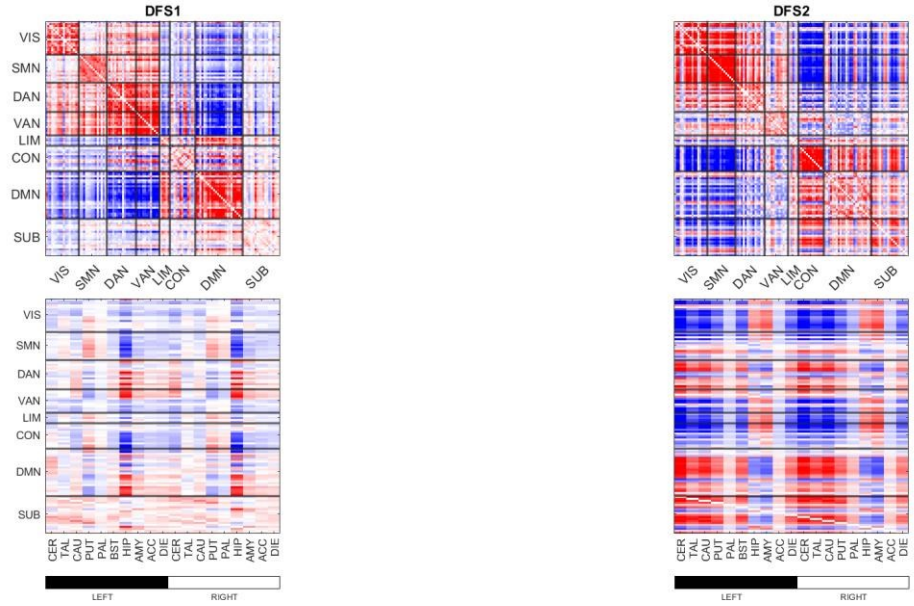

Fig. 17*. Dynamic Functional States obtained with the Schaefer's atlas for K=2.*

4.1.2. Additional comparison

Finally, we provide additional insights into the relationship between the two parcellations by leveraging Principal Component Analysis to investigate the degree of convergence between the two partitions. We show a comparison for different values of K (i.e., K=2 and K=5) between what we displayed in Fig. 12 (Fig. 18a) and the same Gordon Laumann's space but with cluster's indices belonging to Schaefer's partition (Fig. 18b). This visualization allows us to see how the sliding windows of the first clustering were labeled with the new atlas, confirming the shallow coherence of the two parcellations.

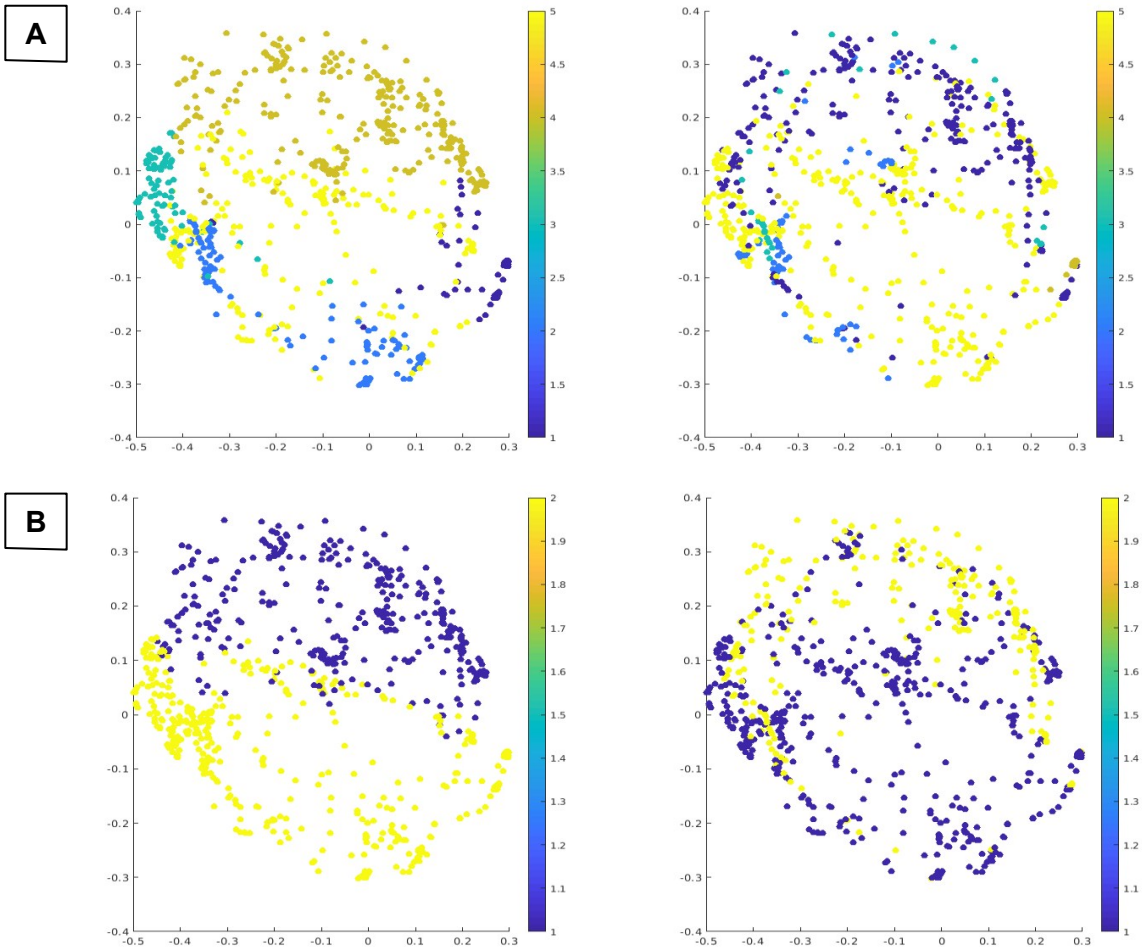

Fig. 18. *First 2 components of a PCA applied to the eigen decomposition of the first subject's time-series for K=5* ***(a)*** *and K=2* ***(b).*** *On the left side the components and the indices are obtained with the Gordon Laumann's parcellation while on the right the indices are from the Schaefer's parcellation.*

4.1.3. Cortico-subcortical activity synchronization

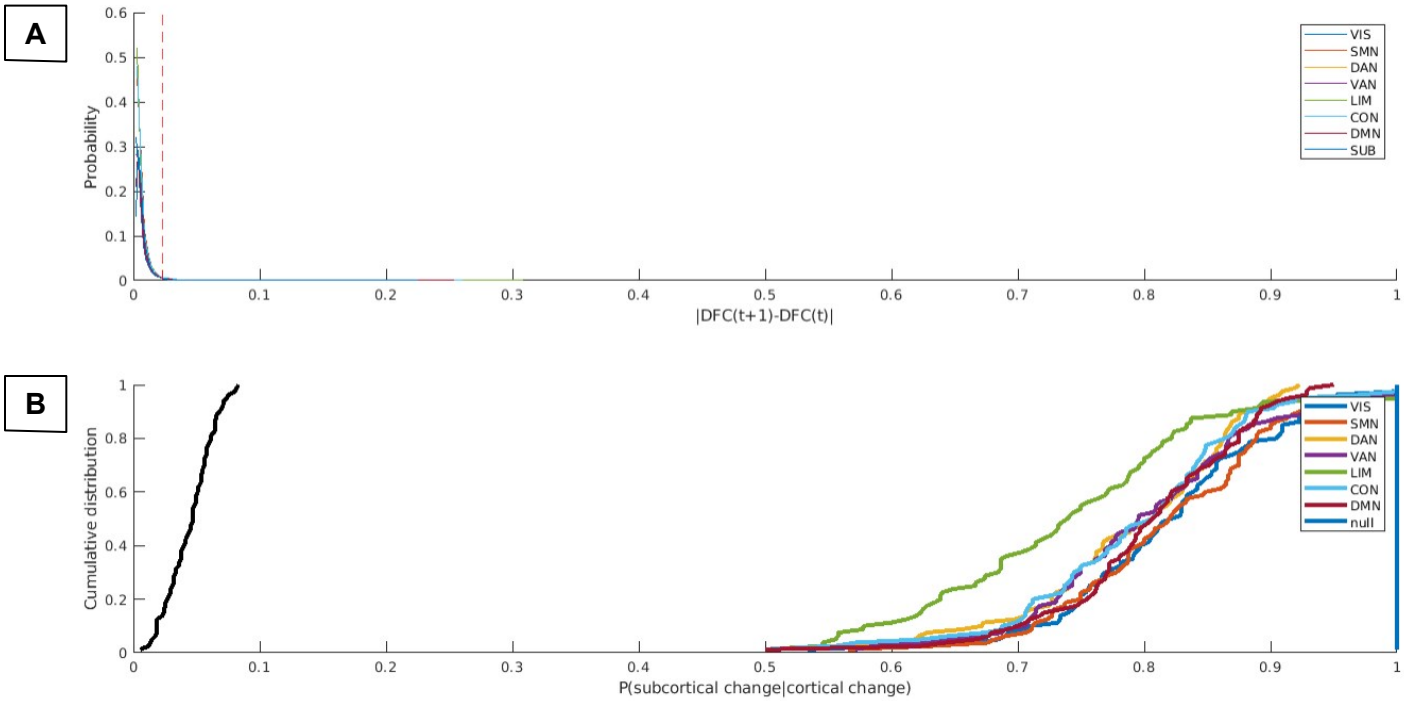

Fig. 19. (a) *Probability distribution of the absolute values of connectivity differences between consecutive sliding windows. Each line represents a different network.* ***(b)*** *Cumulative density function of the conditioned probability of subcortical connectivity reorganization, given a cortical connectivity reorganization. Each colored line indicates a different cortical network. The black line shows the cumulative density function under the null hypothesis of independence between cortical and subcortical changes.*

Another important result that we proved to be invariant both to the dataset and the cortical parcellation was the activity synchronization between cortical and subcortical regions firstly highlighted by Favaretto et al. (2022). Similarly to what we discussed for our replication study, as we can see in Fig. 19b, shifts in connectivity happened simultaneously for cortical and subcortical regions. In fact, the conditioned probability of a subcortical “jump” given a cortical “jump” is significantly higher than the null hypothesis of independence between the two (black line in Fig. 19b).

4.2. Tian's subcortical atlas

As mentioned in the methods, we also decided to include in our analysis a different subcortical parcellation, developed by Tian et al. (2020), maintaining the cortical atlas of the replication study. That was to test the robustness of our results against an alternative choice of subcortical atlas. Specifically, we considered the S1 version (i.e., coarse version with 8 bilateral regions) and left the S4 (i.e., fine grained version with 27 bilateral regions) for future analysis. In this chapter we will briefly review the similarities and differences that we registered with this alternative parcellation.

4.2.1. S1 subcortical parcellation

Unsurprisingly, the choice of subcortical atlas did not significantly alter the aspect of the Dynamic Functional States with respect to the cortical networks, as evident in Fig. 20. This correspondence is quantitatively portraited in the confusion matrix displayed in Fig. 21, where the relative cluster's assignations between the two parcellations are appreciable. Additionally, taking a closer look at cortico-subcortical interactions, reveals that DFS2 and DFS5 preserve the alternating connectivity pattern between the hippocampus and DMN/primary networks (VIS/SMN/AUD) emerged in Favaretto et al. (2022). Once again, DFS2 shows a strong positive hippocampus/DMN correlation paired with a negative coupling between the hippocampus and the primary networks, while the opposite connectivity pattern is observable in DFS5. This supplementary examination allowed us to verify the consistency of these results across different choices of parcellations, as previously demonstrated by Favaretto and colleagues (2022).

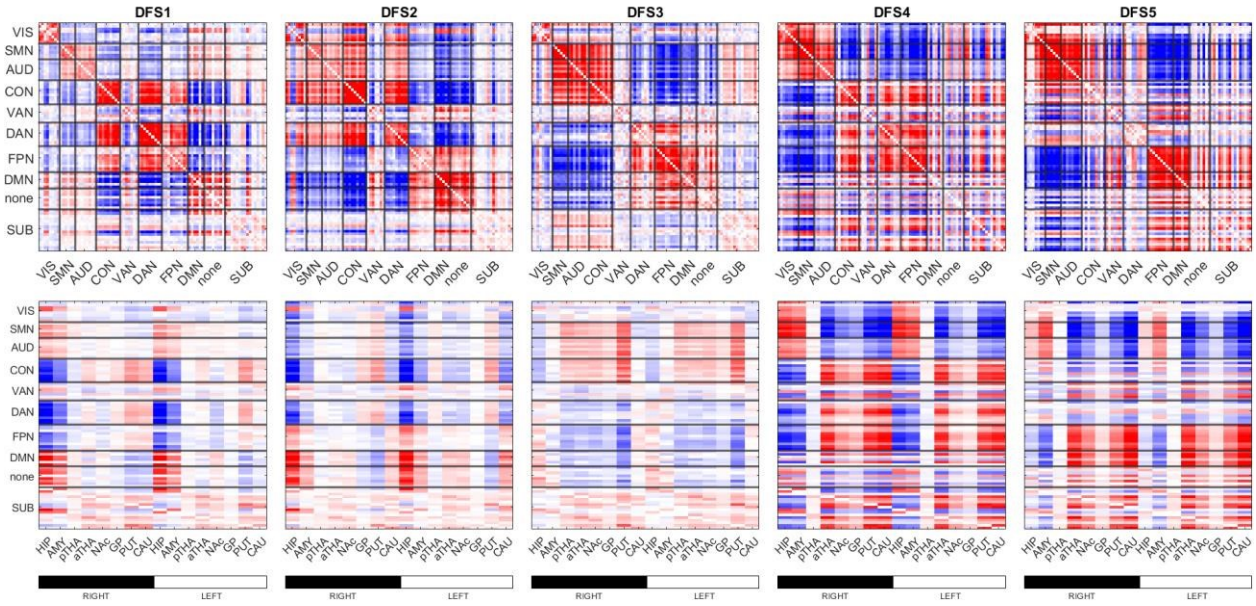

Fig. 20. *Dynamic Functional States obtained with the subcortical atlas developed by Tian et al. (2020).*

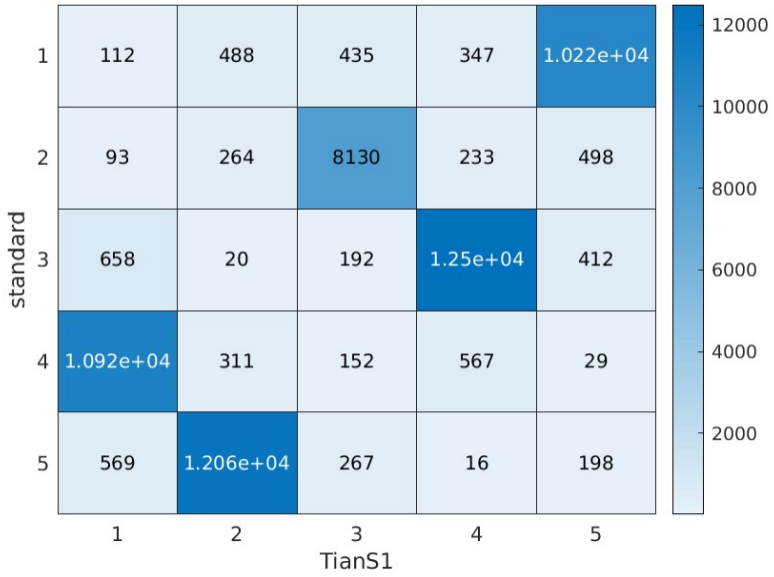

Fig. 21. A confusion matrix with cluster's assignation between the replication analysis conducted with the FreeSurfer subcortical atlas (y axis) and the Tian S1's subcortical atlas (x axis).

5. RESULTS III - Phase randomization

Phase randomization, as many alternative methods (such as ARR), represents a way of testing the results of dFC's analyses against the hypothesis of stationarity of the resting-state fMRI data. Additionally, PR generates null data that are also linear and Gaussian (Liegeois et al., 2017). Consequently, if the surrogate time series generated with this technique does not significantly differ from the original one, it follows that the original data is stationary, Gaussian, and linear.

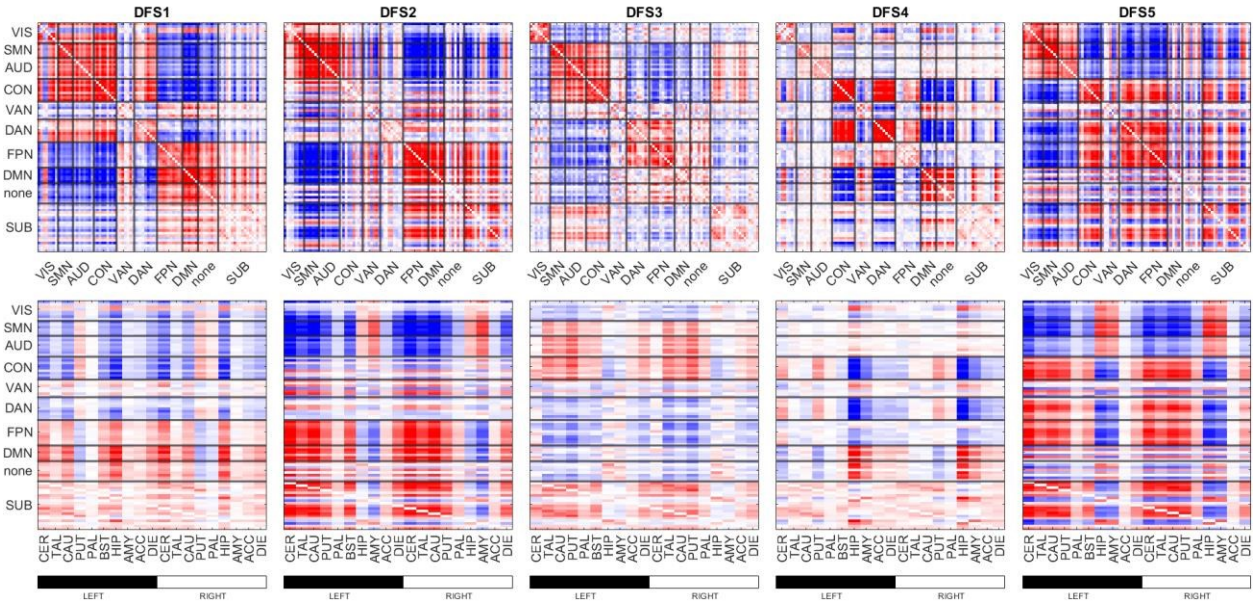

Fig. 22. *Dynamic Functional States obtained with the phase randomization of the original data.*

As evident in Fig. 22, DFSs resulting from the PR-generated time series closely resembles the ones obtained with the original data. This correspondence is furtherly investigated in the confusion matrix represented in Fig. 23. The latter shows a neat one-to-one correspondence between the two sets of clusters, with essentially identical centroids. In other words, clustering phase-randomized data yields the same clusters as

the original data. These results imply that the observed clusters cannot be considered as evidence of nonlinearity, non-stationarity, or non-Gaussianity in the data.

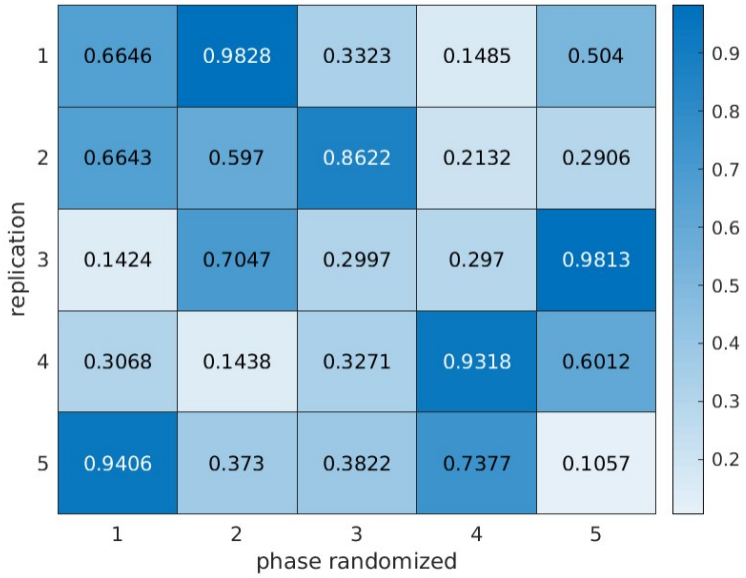

Fig. 23. A confusion matrix with Pearson correlation values for each couple of DFSs between the replication study (y axis) and PR-generated data (x axis).

6. RESULTS IV - Behavioral correlates of dFC

An outstanding question in cognitive neuroscience regards the behavioral implications of dFC. Even though a more rigorous investigation would be required to enrich the state of the art on this matter, here we provide some preliminary efforts substantiating already existing evidence identifying the cognitive domains most strongly influenced by variations in dFC. In this chapter, we try to assess whether fraction or dwell times can significantly predict observed behavioral scores. To this aim, we performed GLM regression using, alternatively, fraction or dwell times as predictors and behavioral indices as dependent variables. We considered five behavioral measures correlated with attentive functions (i.e., MMSE, PSQI, PMAT24, PCPST, SCPT). In particular, we included in the analyses the test's score for the MMSE and the PSQI, the amount of correct answers for the PMAT24 and the PCPST, while for the SCPT we considered the sensitivity score (i.e., the true positive rate, namely the probability of a positive test results in the event of a truly positive occurence) defined as follows:

$$TPR = \frac{TP}{P}$$

where TP is a test result correctly indicating the presence of a condition and P is the number of truly positive cases present in the data. For each GLM model (each behavioral score), we computed the squared Pearson's correlations (R^2) between the observed and the predicted values of the dependent variable. To determine the significance of R^2, we performed a permutation test. We randomly permuted the values of the dependent variable, breaking any statistical association between the dependent and independent variables, which corresponds to the null hypothesis of independence between the

independent and dependent variables. We performed 1000 permutations, recomputing R^2 for each permutation. A p-value was obtained by counting the number of permutations yielding a value of R^2 larger or equal to the value obtained in the non-permuted case.

The first set of predictors we considered was given by the fraction times of the DFSs for each subject, namely the amount of time in which each state was active over the time series of the subject. In Table III we display p-values and R^2 values associated with the corresponding condition. These results suggest that variability in the fraction times had no effect on the behavioral performances that we selected, with p-values never smaller than 0.15.

Table III. *P-value and R-Squared associated with each condition, with fraction times as predictor.*

	SCPT	**PSQI**	**PMAT24**	**PCPST**	**MMSE**
P-value	0.15	0.12	0.79	0.28	0.15
R-Squared	0.08	0.09	0.02	0.06	0.09

In Table IV we display p-values and R-Squared values associated with the corresponding condition, with dwell times as predictors, namely the average length of periods in which each state remains continuously active. Interestingly, among the considered indices, the performance in the Short Penn Continuous Performance Test for measuring sustained attention is the only one that is significantly influenced by the variability in dwell times (p-value=0.007), which explains about the 20% of the variance in the SA's performance (R-Squared=0.21). This result aligns with evidence provided by Liégeois and colleagues

(2019) suggesting that sustained attention is one of the cognitive domains in which dFC explains the largest fraction of variance in task-based performance.

Table IV. *P-value and R-Squared associated with each condition, with dwell times as predictor.*

	SCPT	**PSQI**	**PMAT24**	**PCPST**	**MMSE**
P-value	0.007	0.297	0.927	0.334	0.352
R-Squared	0.21	0.06	0.01	0.06	0.06

7. DISCUSSION AND CONCLUSIONS

The main goal of this thesis was to corroborate the major findings of Favaretto et al. (2022) with data from a different rs-fMRI database (i.e., the one made available by the Human Connectome Project consortium), to consolidate the hypothesis that considers dFC as a multistable connectivity process, strongly influenced by subcortical-cortical connections. Moreover, this work had the additional objective of verifying the robustness of Favaretto et al.'s conclusions (2022) against details of the used methodological pipeline, testing the effects of specific data analysis steps, such as the choice of parcellation or the employment of certain preprocessing procedures. Finally, to expand our understanding of the cognitive relevance of resting-state FC, as suggested by a predictive view of the human brain, we tried to link dFC metrics with aspects of individual behavior.

First of all, the connectivity patterns emerging from our replication study closely resembled the ones described by Favaretto et al. (2022). In particular, the state alternation captured the alternating integration/segregation pattern observed between the hippocampus and DMN/primary networks first observed by Favaretto et al. (2022). Additionally, we lent support to the hypothesis that cortical and subcortical regions interact over time during resting-state conditions, by showing that they exhibit coordinated shifts in connectivity. Importantly, these results were consistent across different choices of cortical and subcortical parcellations. Ultimately, we provided some intriguing, yet preliminary evidence about the possible involvement of resting-state dFC in the

modulation of sustained attention. Below we discuss more specifically these achievements in the subsections 7.1. to 7.3.

7.1. Replication and additional analyses

Finding consistent results across datasets with respect to FC patterns and interactions between specific areas supports the hypothesis that dynamic fluctuations in functional connectivity over time arise as a product of a multistable process, exhibiting shifts between discrete and alternating Dynamic Functional States (DFSs). These DFSs are characterized by different positive/negative correlation patterns among cortical regions and distinctive cortico-subcortical interactions. The alternation between DFSs reflects the flexible arrangement of different cortical networks along a gradient of functional organization (Margulies et al., 2016), having the DMN and the principal networks (VIS/SMN/AUD) at its extremes. A telling example of this flexibility derives from the widely different connectivity patterns exhibited by DFS5 and DFS3 (corresponding respectively to the “old” DFS1 and DFS3 in Favaretto et al., 2022). In DFS5, which aligns with healthy static FC, sensory-motor-attention networks (i.e., VIS, SMN, AUD, CON, DAN) show a strong integration, while being negatively correlated with the DMN. This pattern, encoding the acknowledged separation between task-negative and task-positive networks (Fox et al., 2005), is consistent with the observed interaction between cortical and subcortical networks. DFS5 indeed, is characterized by a positive correlation between DMN and the hippocampus, which in turn is negatively correlated with sensory-motor-attention networks (SMA). On the contrary, in DFS3 the hippocampus exhibits a negative

correlation with the DMN and a positive correlation with SMA networks. The remaining states depict alterations to this pattern, involving adjustments in certain networks along the principal gradient, resulting in a fluctuating balance between integration and segregation. This function of the hippocampus as a mediator in the DMN/SMA networks interaction is consistent with the emerging role of this limbic region as a major hub of functional connectivity organization at a whole-brain level. The hippocampus, in fact, is reportedly identified as having a pivotal role in coordinating the activity of cortical networks at rest (Cole et al., 2010; Chan et al., 2017). For these reasons, our findings support the speculation of Favaretto and colleagues (2022) that one of the hippocampus's functional roles might be to aid switches between alternative patterns of cortical activation. Importantly, we also confirmed that significant transitions in connectivity (identified as large connectivity reorganizations) happen synchronously between cortical and subcortical networks, highlighting their interaction over time. Altogether, these results hint at the relevance of subcortical connectivity in the coordination of cortical and large-scale whole-brain dynamics, remarking the necessity of thoroughly considering the influence of cortico-subcortical interaction when building connectivity-based models of brain activity at rest. Additionally, we suggest to further investigate the relationship with subcortical networks by exploiting more detailed parcellations, such as the fine-grained versioned proposed by Tian and colleagues (2020).

An important advancement of this study with respect to the one conducted by Favaretto et al. (2022) consists in a stronger validation of the methodological pipeline. In our study, we carefully considered the effects and implications of each preprocessing step. In particular, we showed that both the distance metric for the clustering and the down-

sampling we applied to compensate for the difference in TR between the Washington University and the HCP's dataset had virtually no effect on the aspect of the states. However, avoiding the application of Global Signal Regression (GSR) on the data, dramatically affected the appearance of the resulting DFSs both at a qualitative and at a quantitative level. Given its strong impact, GSR is a debated practice in the analysis of fMRI's data (Nalci et al., 2017). Hence, we recommend a critical approach when including this preprocessing step, paired with a detailed investigation of its consequences on rs-fMRI data. Importantly, as previously highlighted by Favaretto and colleagues (2022), the results we discussed in this section were invariant to the choice of parcellation (both cortical and subcortical).

7.2. Phase randomization

Results of phase randomization showed an exhaustive correspondence between the original and the PR-generated data. These findings led us to conclude that the evidence of a time-varying connectivity, captured by the existence of different DFSs, is not sufficient to exclude the linearity, Gaussianity or stationarity of our data. Had we obtained the opposite finding, namely, that temporal variations in resting-state FC are due to a non-stationarity of the process, we would exclude that the dynamic component of FC emerges as a mere consequence of sampling variability. Our findings, however, do not lead us to conclude that dFC is entirely spurious. They only suggest some caution in the interpretation of the DFSs. According to a strict statistical definition of stationarity, signals that are extensively considered to encode dFC (e.g., data generated by Hidden Markov Models) are fully stationary. Thus, we do not conclude that there is no true temporal variability in connectivity. However, stationarity and linearity together imply that the distinct DFSs cannot be identified with multiple dynamical attractors of non-linear dynamics. Thus, what we showed in this chapter suggests the necessity of further investigations regarding the interpretation of the observed clusters. In particular, it will be interesting to relate the DFSs to complex trajectories in FC space (Battaglia et al., 2020).

7.3. Behavioral implications

Our preliminary analysis about potential behavioral correlates of dFC, revealed a significant effect of interindividual differences in the average continuative activity of the states (i.e., dwell times) on the performance of a sustained attention test. In particular, we assessed the impact of variations in the dwell times on the sensitivity score associated to the Number/Letter version of the Short Penn Continuous Performance Test (Gur, 2010). We registered that our predictor explained about 20% of the variability in the sensitivity values for the SCPT (R-Squared=0.21). This result tells us that the dwell times associated to the DFSs are associated with a modulation of the performance in sustained attention's tasks. A potential explanation for this effect might be that individuals exhibiting lower dwell times, resulting in faster transitions between the states, are more capable of effectively adapting to rapidly changing and uncertain environments (such as the ones object of standard SA's test). Future investigations should include larger samples and consider alternative sustained attention indices. Additionally, to fully address the challenge of revealing the behavioral implications of dFC, it would be important to demonstrate causal links between static/dynamic FC and behavior, going beyond current literature that mostly presents purely correlative findings. A promising way to causally modulate static/dynamic FC might combine non-invasive brain stimulation with recent advancements in network control theory (Kamiya et al., 2023; Deco et al., 2019) to design an experiment allowing to modulate specific FC links with a supposed relevance for the cognitive domain of interest and observing its effects on behavioral performance.

BIBLIOGRAPHY

Albert, N.B., Robertson, E.M., Miall, R.C., (2009). The resting human brain and motor learning. *Current Biology.* 19(12), 1023-1027.

Alle H., Roth A., Geiger J.R., (2009). Energy-efficient action potentials in hippocampal mossy fibres. *Science* 325, 1349–51

Allen, E.A., Damaraju, E., Plis, S.M., et al., (2014). Tracking whole-brain connectivity dynamics in the resting state. *Cerebral Cortex.* 24(3), 663-676.

Baldassarre, A., Ramsey, L., Rengachary, J., et al., (2016). Dissociated functional connectivity profiles for motor and attention deficits in acute right-hemisphere stroke. *Brain.* 139(7), 2024-2038.

Battaglia, D., Boudou, T., Hansen, E. C., et al., (2020). Dynamic functional connectivity between order and randomness and its evolution across the human adult lifespan. *NeuroImage*, *222*, 117-156.

Baudouin, A., Clarys, D., Vanneste, S., Isingrini, M., (2009). Executive functioning and processing speed in age-related differences in memory: Contribution of a coding task. *Brain and Cognition.* 71 (3), 240–245.

Bilker, W.B., Hansen, J.A., Brensinger, C.M., et al., (2012). Development of Abbreviated Nine-Item Forms of the Raven's Standard Progressive Matrices Test. *Assessment*. 19(3), 354–369.

Bruckmaier, M., Tachtsidis, I., Phan, P., et al., (2020). Attention and capacity limits in perception: a cellular metabolism account. *Journal of Neuroscience.* 26;40(35), 6801-6811.

Buysse, D.J., Reynolds, C.F. 3rd, Monk, T.H., et al., (1989). The Pittsburgh Sleep Quality Index: a new instrument for psychiatric practice and research. *Psychiatry Research.* 28(2), 193-213.

Carlozzi, N.E., Beaumont, J.L., Tulsky, D.S., Gershon, R.C., (2005). The NIH Toolbox Pattern Comparison Processing Speed Test: Normative Data. *Archives of Clinical Neuropsychology.* 30(5), 359-68.

Carter B.C., Bean B.P., (2009). Sodium entry during action potentials of mammalian neurons: incomplete inactivation and reduced metabolic efficiency in fast-spiking neurons. *Neuron.* 64, 898–909

Chan, R.W., Leong, A.T.L., Ho, L.C., et al., (2017). Low-frequency hippocampal-cortical activity drives brain-wide resting-state functional MRI connectivity. *Proceedings of the National Academy of Sciences of the U.S.A*. 114(33), E6972-E6981.

Chiaravalloti, N.D., Christodoulou, C., Demaree, H.A., DeLuca, J. (2003). Differentiating simple versus complex processing speed: Influence on new learning and memory performance. *Journal of Clinical and Experimental Neuropsychology*. 25 (4), 489–501.

Cole, M.W., Pathak, S., Schneider, W., (2010). Identifying the brain's most globally connected regions. *NeuroImage*. 49(4), 3132-48.

Crum, R.M., Anthony, J.C., Bassett, S.S., Folstein, M.F., (1993). Population-based norms for the Mini-Mental State Examination by age and educational level. *Journal of the American Medical Association*. 269(18), 2386-2391.

Damoiseaux, J.S., Greicius, M.D., (2009). Greater than the sum of its parts: a review of studies combining structural connectivity and resting-state functional connectivity. *Brain Structure and Function*. 213, 525–533

Damoiseaux, J.S., Rombouts, S.A.R.B., Barkhof, F., et al., (2006). Consistent resting-state networks across healthy subjects. *Proceedings of the National Academy of Sciences of the U.S.A.* 103, 13848–13853.

Deco, G., Cruzat, J., Cabral, J., et al., (2019). Awakening: Predicting external stimulation to force transitions between different brain states. *Proceedings of the National Academy of Sciences of the U.S.A*. 116(36), 18088-18097.

Duncan, J., (2003). Intelligence tests predict brain response to demanding task events. *Nature Neuroscience*. 6, 207–208.

Duncan, J., (2005). Frontal Lobe Function and General Intelligence: Why it Matters. *Cortex.* 41(2), 215-217.

Duncan, J., Seitz, R.J., Kolodny, J., Bor, D., et al., (2000). A neural basis for general intelligence. *Science*. 289(5478), 457-460.

Favaretto, C., Allegra, M., Deco, G., et al., (2022). Subcortical-cortical dynamical states of the human brain and their breakdown in stroke. *Nature Communications.* 13, 5069.

Fischl, B., (2012). FreeSurfer. *NeuroImage*62, 774–781.

Fischl, B., Salat, D.H., Busa, E., Albert, M., et al., (2002). Whole brain segmentation: automated labelling of neuroanatomical structures in the human brain. *Neuron.* 33, 341–355.

Folstein, M.F., Folstein, S.E., McHugh, P.R., (1975). "Mini-mental state". A practical method for grading the cognitive state of patients for the clinician. *Journal of Psychiatric Research.* 12(3), 189-198.

Foster, D.J., (2017). Replay comes of age. *Annual Review of Neuroscience.* 40, 581-602.

Fox, M.D., Snyder, A.Z., Vincent, J.L., et al., (2005). The human brain is intrinsically organized into dynamic, anticorrelated functional networks. *Proceedings of the National Academy of Sciences of the U.S.A*. 102(27), 9673-9678.

Glasser, M.F., Sotiropoulos, S.N., Wilson, J.A., Coalson, T.S., et al., (2013). The minimal preprocessing pipelines for the Human Connectome Project. *NeuroImage.* 15(80), 105-124.

Gordon, E.M., Laumann, T.O., Adeyemo, B., et al., (2016). Generation and evaluation of a cortical area parcellation from resting-state correlations. *Cerebral Cortex.* 26(1), 288-303.

Gur, R.E., (2010). A cognitive neuroscience-based computerized battery for efficient measurement of individual differences: standardization and initial construct validation. *Journal of Neuroscience Methods.* 187 (2), 254–262.

Harris, J.J., Jolivet, R., Attwell, D., (2012). Synaptic energy use and supply. *Neuron.* 75(5), 762-777.

Howarth, C., Gleeson, P., Attwell, D., (2012). Updated energy budgets for neural computation in neocortex and cerebellum. *Journal of Cerebral Blood Flow & Metabolism.* 32, 1222-1232.

Hutchison, R.M., Womelsdorf, T., Allen, E.A., et al., (2013). Dynamic functional connectivity: promises, issues and interpretations. *NeuroImage.* 80, 360-378.

Kamiya, S., Kawakita, G., Sasai, S., et al., (2023). Optimal control costs of brain state transitions in linear stochastic systems. *Journal of Neuroscience.* 43(2), 270-281.

Leonardi, N., Van De Ville, D., (2015). On spurious and real fluctuations of dynamic functional connectivity during rest. *NeuroImage.* 104, 430-436.

Liégeois, R., Laumann, T. O., Snyder, A. Z. et al., (2017). Interpreting temporal fluctuations in resting-state functional connectivity MRI. *NeuroImage.* 163, 437–455.

Liégeois, R., Li, J., Kong, R. et al*.,* (2019). Resting brain dynamics at different timescales capture distinct aspects of human behavior. *Nature Communication.* 10, 2317.

Margulies, D.S., Ghosh, S.S., Goulas, A., et al., (2016). Situating the default-mode network along a principal gradient of macroscale cortical organization. *Proceedings of the National Academy of Sciences of the U.S.A*. 113, 12574–12579.

Mayes, S.D., Calhoun, S.L. (2007). Learning, attention, writing, and processing speed in typical children and children with ADHD, autism, anxiety, depression, and oppositional-defiant disorder. *Child Neuropsychology.* 13 (6), 469–493.

Mink, J.W., Blumenschine, R.J., Adams, D.B., (1981). Ratio of central nervous system to body metabolism in vertebrates: its constancy and functional basis. *American Journal of Physiology.* 241, 203–212.

Nalci, A., Rao, B.D., Liu, T.T., (2017). Global signal regression acts as a temporal downweighting process in resting-state fMRI. *NeuroImage.* 152, 602-618.

Petersen, S.E., Fox, P.T., Posner, M.I., et al., (1988). Positron emission tomographic studies of the cortical anatomy of single-word processing. *Nature.* 331, 585-589.

Pezzulo, G., Zorzi, M., Corbetta, M., (2021). The secret life of predicitive brains: what's spontaneous activity for? *Trends in Cognitive Sciences.* 25(9), 730-743.

Prabhakaran, V., Smith, J.A., Desmond, J.E., et al., (1997). Neural substrates of fluid reasoning: an fMRI study of neocortical activation during performance of the Raven's Progressive Matrices Test. *Cognitive Psychology.* 33(1), 43-63.

Raichle, M.E., (2010). Two views of brain function. *Trends in Cognitive Sciences,* 14(4), 180-190.

Romano, S., Bailey, J., Nguyen, V., Verspoor, K., (2014). Standardized Mutual Information for Clustering Comparisons: One Step Further in Adjustment for Chance. *Proceedings of Machine Learning Research*. 32(2), 1143-1151.

Sarter, M., Givens, B., Bruno, J.P., (2001). The cognitive neuroscience of sustained attention: where top-down meets bottom-up. *Brain Research Reviews*. 35(2), 146-160.

Smith, S.M., Nichols, T.E., Vidaurre, D., et al., (2015). A positive-negative mode of population covariation links brain connectivity, demographics and behavior. *Nature Neuroscience.* 18, 1565-1567.

Sokoloff, L., Mangold, R., Wechsler, R.L., et al., (1955). The effect of mental arithmetic on cerebral circulation and metabolism. *Journal of Clinical Investigation.* 34(7), 1101-1108.

Tian, Y., Margulies, D.S., Breakspear, M., et al., (2020). Topographic organization of the human subcortex unveiled with functional connectivity gradients. *Nature Neuroscience.* 23, 1421-1432.

Uddin, L.Q., Yeo, B.T.T., Spreng, R.N., (2019). Towards a universal taxonomy of macro-scale functional human brain networks. *Brain Topography.* 32(6), 926-942.

Van Essen, C.D., Smith, M.S., Barch M.D., et al., (2013). The WU-Minn Human Connectome Project: an overview. *NeuroImage.* 80, 62-79.

WU-Minn HCP. (2017). 1200 Subjects Data Release Reference Manual.